Check for updates

JGR Oceans

RESEARCH ARTICLE
10.1029/2023JC020799

Atmospheric Forcing Dominates the Interannual Variability of Convection Strength in the Irminger Sea

M. F. de Jong[1], K. E. Fogaren[2], I. Le Bras[3], L. McRaven[3], and H. I. Palevsky[2]

[1]Department of Ocean Systems, Royal Netherlands Institute for Sea Research (NIOZ), Texel, The Netherlands, [2]Boston College, Morrissey College of Arts and Sciences, Chestnut Hill, MA, USA, [3]Woods Hole Oceanographic Institution, Woods Hole, MA, USA

Abstract Transformation of light to dense waters by atmospheric cooling is key to the Atlantic Meridional Overturning Circulation in the Subpolar Gyre. Convection in the center of the Irminger Gyre contributes to the formation of the densest waters east of Greenland. We present a 19-year (2002–2020) weekly time series of hydrography and convection in the central Irminger Sea based on (bi-)daily mooring profiles supplemented with Argo profiles. A 70-year annual time series of shipboard hydrography shows that this mooring period is representative of longer-term variability. The depth of convection varies strongly from winter to winter (288–1,500 dbar), with a mean March mixed layer depth (MLD) of 470 dbar and a mean maximum density reached of 27.70 ± 0.05 kg m^{-3}. The densification of the water column by local convection directly impacts the sea surface height in the center of the Irminger Gyre and thus large-scale circulation patterns. Both the observations and a Price-Weller-Pinkel mixed layer model analysis show that the main cause of interannual variability in MLD is the strength of the winter atmospheric surface forcing. Its role is three times as important as that of the strength of the maximum stratification in the preceding summer. Strong stratification as a result of a fresh surface anomaly similar to the one observed in 2010 can weaken convection by approximately 170 m on average, but changes in surface forcing will need to be taken into account as well when considering the evolution of Irminger Sea convection under climate change.

Plain Language Summary The Atlantic circulation brings warmer, lighter waters northwards in the upper part of the ocean, and colder, denser waters southward in the lower part of the ocean, creating a stable, stratified water column. East of Greenland, in the Irminger Sea, cooling by the atmosphere can transform these warm, lighter waters into the denser, deeper waters, which will eventually mix with deeper waters and flow southwards. To better understand how this transformation works and varies from year to year, we study measurements from instruments moored throughout the water column in the Irminger Sea between 2002 and 2020. We describe the progression of the average winter transformation and examine why transformation is stronger in some winters than in others. Overall, we find that the strength of winter cooling is three times as important as the stability of the water column, a measure of its resistance to transformation, in the summer before. This finding will be important to better predict how the Atlantic circulation will develop in the future as a result of climate change.

Key Points:

- A 19-year data set compiled from moorings and Argo floats shows that convection varied from 300 to 1,500 dbar from 2002 to 2020
- Convection since the winter of 2014–2015 has cooled and freshened the central Irminger Sea
- Atmospheric forcing is three times as important as stratification in determining the maximum mixed layer depth

Supporting Information:

Supporting Information may be found in the online version of this article.

Correspondence to:

M. F. de Jong,
femke.de.jong@nioz.nl

Citation:

de Jong, M. F., Fogaren, K. E., Le Bras, I., McRaven, L., & Palevsky, H. I. (2025). Atmospheric forcing dominates the interannual variability of convection strength in the Irminger Sea. *Journal of Geophysical Research: Oceans*, *130*, e2023JC020799. https://doi.org/10.1029/2023JC020799

Received 7 DEC 2023
Accepted 16 DEC 2024

Author Contributions:

Conceptualization: M. F. de Jong, H. I. Palevsky
Data curation: M. F. de Jong, I. Le Bras, L. McRaven
Formal analysis: M. F. de Jong
Funding acquisition: M. F. de Jong
Investigation: M. F. de Jong
Methodology: M. F. de Jong, K. E. Fogaren
Project administration: M. F. de Jong
Resources: M. F. de Jong, K. E. Fogaren, I. Le Bras, L. McRaven, H. I. Palevsky
Software: M. F. de Jong, K. E. Fogaren
Supervision: M. F. de Jong
Validation: M. F. de Jong
Visualization: M. F. de Jong
Writing – original draft: M. F. de Jong

© 2025. The Author(s).
This is an open access article under the terms of the Creative Commons Attribution License, which permits use, distribution and reproduction in any medium, provided the original work is properly cited.

1. Introduction

Deep convection, the process by which buoyant surface waters are transformed into denser waters by surface cooling (Marshall & Schott, 1999), is important for the Atlantic Meridional Overturning Circulation (AMOC). Eventually, through sinking along the boundaries (Katsman et al., 2018), these dense waters contribute to the Deep Western Boundary Current, which forms the deep southward branch of the AMOC. In model studies, the changes in strength of convection in the Subpolar Gyre are often linked to changes in AMOC strength, with many studies focused on deep convection in the Labrador Sea (Böning et al., 2006; Eden & Willebrand, 2001; Woods et al., 1999; Zhang et al., 2019).

Since 2014, the strength of the AMOC in the Subpolar Gyre has been measured by the Overturning in the Subpolar North Atlantic Program (OSNAP) array (Li et al., 2021; Lozier et al., 2017, 2019). The OSNAP array consists of two legs, OSNAP West crosses the Labrador Sea from Canada to Greenland and OSNAP East extends from Greenland eastward through the Irminger Sea, Iceland Basin and Rockall Trough to the European shelf. The results from OSNAP show that the eastern basins contribute most to both the total overturning strength as well as

Writing – review & editing:
M. F. de Jong, K. E. Fogaren, I. Le Bras, L. McRaven, H. I. Palevsky

the variability of the overturning (Li et al., 2021; Lozier et al., 2019). Petit et al. (2020) showed that the subpolar overturning strength is linked to water-mass transformation by surface forcing over the Irminger and Iceland basins. Chafik et al. (2022) found that the link between Irminger Sea density and AMOC strength observed in the mooring data also existed in a longer (1993–2018) reanalysis time series and deemed the Irminger Sea to be the center of action for the subpolar AMOC. Furthermore, it is not the boundary currents that contribute most to the variability in OSNAP East, but the open-ocean basins (Li et al., 2021).

The density in the Irminger Sea is strongly affected by local convection. The occurrence of deep convection in the Irminger Sea was mentioned originally by Nansen (1912) and Sverdrup et al. (1942). After a long period of disinterest, the causes of which are detailed by Pickart et al. (2003), convection in the Irminger Sea received renewed attention with a series of studies on eventful convection years in the 2000s (de Jong & de Steur, 2016; de Jong et al., 2012, 2018; Piron et al., 2015, 2017). These studies used data from moorings in the CIS as well as Argo data to determine mixed layer depths. They showed that convection down to depths of 1,600 m can occur and that convection is mainly driven by strong winter air-sea heat fluxes. Longer time series of near-annually sampled hydrographic data (van Aken et al., 2011) paint a similar picture, with evidence of strong convection seen in oxygen concentrations and Potential Vorticity (PV) in the Irminger Sea during periods of strong positive North Atlantic Oscillation (NAO), similar to findings for deep convection in the Labrador Sea (van Aken et al., 2011; Yashayaev, 2007). Josey et al. (2019) proposed that a combination of a positive NAO and an East Atlantic Pattern, which is weaker than the NAO, is linked to a higher occurrence of tip jets over the Irminger Sea (Moore, 2003; Moore & Renfrew, 2005) and therefore is linked to strong local winter cooling.

However, strong surface forcing does not necessarily equate to strong convection. There have been periods in the observed record when convection was suppressed in the Labrador Sea by strong surface stratification during periods of strong surface forcing (Belkin et al., 1998; Gelderloos et al., 2012). Anomalously fresh near-surface layers, termed Great Salinity Anomalies (GSA), were suggested to suppress convection in the Labrador Sea from 1968 to 1972 (Lazier, 1980) and from 1981 to 1985 (Dickson et al., 1988; Straneo, 2006; van Aken et al., 2011). However, the GSA of the 1970s was recently revisited by Kim et al. (2021), and their model simulations show that reduced surface fluxes may have had a larger role in the reduction of convection than the anomalously strong stratification. The GSA were advected around the Subpolar Gyre and were also observed in the Irminger Sea by van Aken et al. (2011), who suggest that despite the salinity anomaly, some moderate convection may have occurred in the Irminger Sea in the early 1980s. The first analysis on the effect of a recent fresh anomaly on the stratification in the Irminger Sea by Bilo et al. (2022) found that the anomaly must have contributed partially to the weaker convection in the winter of 2019. Furthermore, the stratification in the region is projected to increase due to global warming and increased freshwater input from Greenland's Ice Sheet (Bakker et al., 2016; Sgubin et al., 2017). Thus, Irminger Sea convection may be inhibited by strong stratification more often or even permanently, potentially weakening the subpolar AMOC, which would have consequences for climate around the North Atlantic (Boning et al., 2016). It is therefore important to understand the variability of convection in this important region of the Subpolar Gyre and its dependence on surface forcing and stratification.

This paper aims to present a comprehensive description of convection in the CIS and its variability, and the causes of variability, based on a high temporal resolution multi-mooring time series supplemented with Argo records. The mooring time series covers the period from 2002 to 2020, which includes both periods of weak (mixed layers <500 m) and strong (mixed layers >1,000 m) convection. We then place this 19-year record in a longer term context using a multi-decadal time series from near-annual hydrographic sections from 1950 to 2020. The relative importance of atmospheric forcing versus stratification as driving forces of Irminger Sea convection strength variability is investigated using the mooring data as well as results from the one dimensional Price, Weller, Pinkel (PWP, Price et al., 1986) mixed layer model.

Section 2 presents the data sets used in this study and details the processing methods. In Section 3, we provide the comprehensive description of Irminger Sea convection and hydrography, with a focus on the seasonal climatology based on the 19-year time series in Section 3.1 and a focus on the interannual variability in Section 3.2. In Section 4 we present the attribution of the variability, specifically the role of ocean stratification versus atmospheric forcing. Section 4.1 uses the mooring-Argo time series for a first attribution and in Section 4.2 we investigate the role of stratification versus surface buoyancy forcing in more detail using the PWP model. Section 5 contains the discussion and conclusions.

21699291, 2025, 2, Downloaded from https://agupubs.onlinelibrary.wiley.com/doi/10.1029/2023JC020799, Wiley Online Library on [31/01/2025]. See the Terms and Conditions (https://onlinelibrary.wiley.com/terms-and-conditions) on Wiley Online Library for rules of use; OA articles are governed by the applicable Creative Commons License

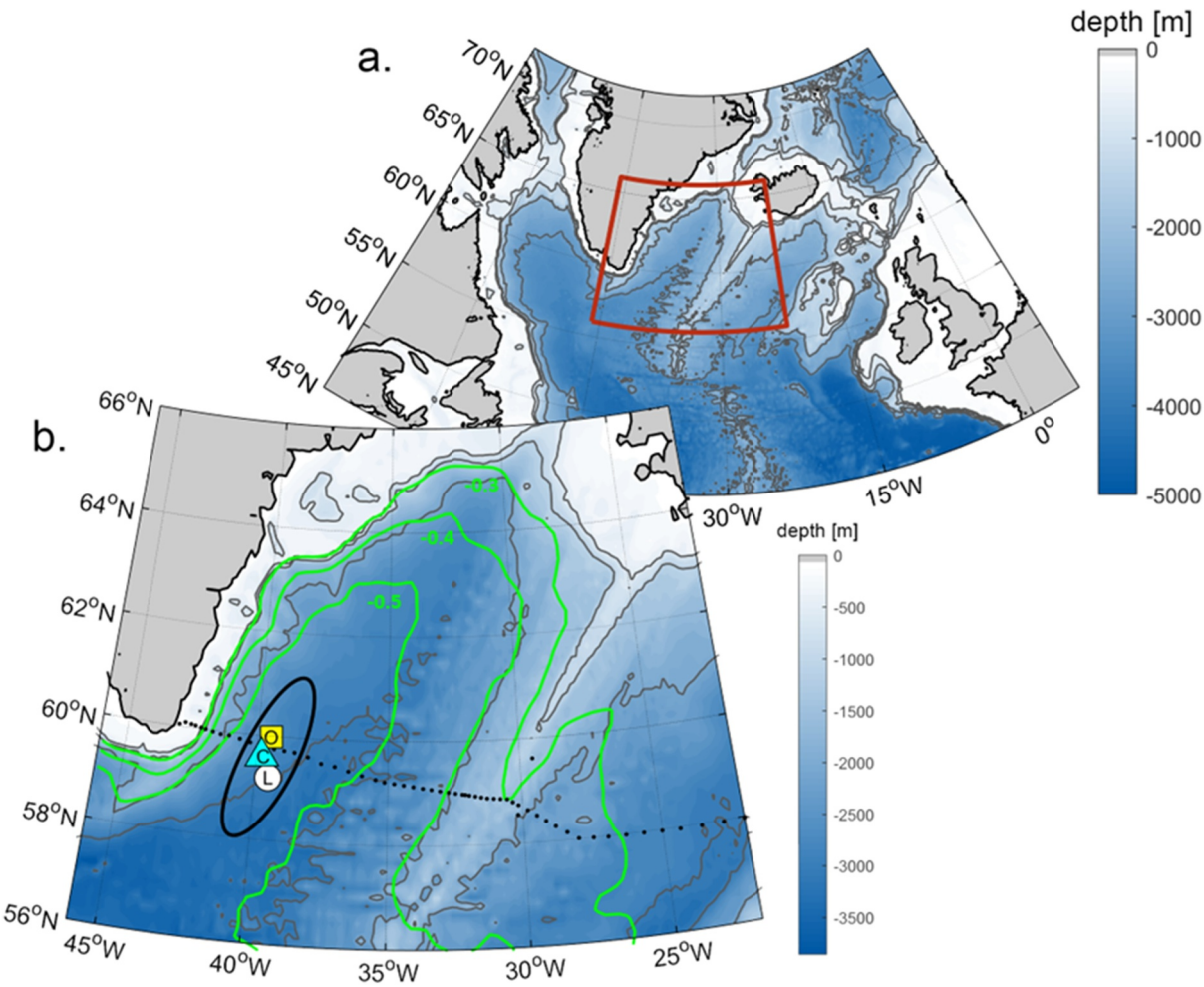

Figure 1. Maps of the study area and mooring locations. (a) Overview map of the bathymetry of the northern North Atlantic. The Irminger Sea is enclosed by the red box. (b) Zoom in of the red box with mooring locations in the Central Irminger Sea (CIS) indicated; white circle for Long-term Ocean Circulation Observations, yellow square for Ocean Observatories Initiative, cyan triangle for CIS and black dots indicate a typical CTD transect along the Overturning in the Subpolar North Atlantic Program array. Argo profiles were collected within the area enclosed by the black ellipse. Sea surface height (m) contours are plotted in green at 10 cm intervals.

2. Data and Methods

2.1. Hydrographic Profile Data From Moorings and Argo Floats

The record presented here is composed of data sets from four different programs in the CIS: the Long-term Ocean Circulation Observations (LOCO) mooring, the profiling HYPM mooring of the Ocean Observatories Initiative (OOI), the Central Irminger Sea (CIS) mooring, and the Argo profiles around these three moorings (Figure 1). These platforms sampled the upper 2 km of the water column and partially overlap in time. However, each of them have data gaps in time and space (Figure S1 in Supporting Information S1), making it necessary to merge them into one complete record.

The LOCO mooring, maintained from summer 2003 through summer 2018 by the Royal Netherlands Institute for Sea Research, was located in the center of the cyclonic circulation of the Irminger Gyre at approximately 59.2°N and 39.5°W (Figure 1; de Jong & de Steur, 2016; de Jong et al., 2012, 2018). The OOI observatory in the Irminger Sea consists of four moorings. Here we use the data from the OOI HYPM profiling mooring (de Jong et al., 2018), which is located slightly to the north of the LOCO position at 60°N and 39.5°W. The OOI profiler record presented here covers the 2014 to 2020 period. Both the LOCO and OOI HYMP mooring were outfitted with a McLane moored profiler (MMP) that records CTD (conductivity, temperature, depth) profiles at high vertical resolution along the mooring cable in the 150–2,400 m interval for LOCO and the 230–2,500 m interval for OOI.

21699291, 2025, 2, Downloaded from https://agupubs.onlinelibrary.wiley.com/doi/10.1029/2023JC020799, Wiley Online Library on [31/01/2025]. See the Terms and Conditions (https://onlinelibrary.wiley.com/terms-and-conditions) on Wiley Online Library for rules of use; OA articles are governed by the applicable Creative Commons License

21699291, 2025, 2, Downloaded from https://agupubs.onlinelibrary.wiley.com/doi/10.1029/2023JC020799, Wiley Online Library on [31/01/2025]. See the Terms and Conditions (https://onlinelibrary.wiley.com/terms-and-conditions) on Wiley Online Library for rules of use; OA articles are governed by the applicable Creative Commons License

The time resolution for the MMP profiles varies from several times per day (LOCO deployment in summer 2011) to daily (other LOCO deployments) to every 20 hr (for OOI). For the OOI MMP data, paired upwards and downwards profiles are averaged prior to analysis to remove hysteresis effects, yielding one mean profile every 40 hr. Detailed data processing and quality control of the MMP data is described in de Jong et al. (2012). Special care is taken to correct for sensor drift of the conductivity sensor over the deployment using shipboard CTD data in order to obtain a consistent salinity record over the whole period.

The CIS mooring, located between the LOCO and OOI moorings at 59.5°N and 39.8°W, was maintained by GEOMAR from 2002 to 2016. It was outfitted with instruments at fixed depths (de Jong et al., 2018) rather than a moving platform like the MMP. As a result, the daily CIS profiles have a lower vertical resolution than the LOCO and OOI moorings, allowing for less accuracy in determining stratification and especially in locating the bottom of the mixed layers in winter. Therefore, we mainly use the CIS mooring data when no higher-resolution profiles are available. This is primarily in 2002–2003 before the start of the LOCO deployment and at times when there are gaps in the records of the higher-resolution LOCO and OOI moorings (Figure S1 in Supporting Information S1).

Argo float profiles, with similar vertical resolution of the MMP profilers, were used to provide data in the near surface layer of the water column not covered by the MMPs. Argo profiles were selected in an ellipse around the center of the mooring positions, with a long axis distance of twice the north-south distance between the OOI and LOCO moorings, and a short axis of twice the east-west distance between these two moorings (Figure 1). The ellipse is aligned with the continental shelf of Greenland and the sea surface height contours, which ensures that the data represents changes over time in the weakly stratified central Irminger Gyre and excludes spatial differences arising from the more buoyant boundary currents. Argo floats typically record a profile every 10 days, but the amount of profiles in the study area depends on the number of floats present in the Irminger Sea each year. Over the years 2003–2020 there were on average 34 ± 21 (standard deviation) profiles per year recorded in the area enclosed by the ellipse. More details on the number of available mooring and Argo profiles is presented in supporting information S1.

We composed a merged multi-mooring/Argo record to investigate hydrographic changes in the CIS over the 2002–2020 period. This record was constructed as follows. Absolute salinity (SA), conservative temperature (CT) and potential density with respect to the surface (σ_0) were derived using the TEOS-10 toolbox (www.teos-10.org). Individual SA and CT profiles were subsampled vertically by averaging within 25 dbar intervals, which is a lower resolution than both the mooring and Argo profiles, and is done to make the profiles comparable. Next, profiles were averaged in time by applying a 1-week moving window. If LOCO, OOI or Argo profiles were available only these were used, otherwise the lower vertical resolution CIS data (when available) was used. This vertical and temporal smoothing removed small differences between the profiles that originate from their offset locations, while maintaining the subseasonal, seasonal and interannual variability that we are interested in. Choosing a time window smaller than a week would have resulted in more gaps. The resulting weekly profiles in this merged record were extended to the surface using (a) sea surface temperature (SST) data from the fifth generation European Centre for Medium-Range Weather Forecasts atmospheric reanalysis product (ERA5 SST, a product based on both satellite data and in situ data), (b) a salinity time series based on the upper 50 m of Argo profiles, and (c) salinity and temperature records starting in 2014 from the near-surface instruments (12 m) at the OOI SUMO mooring, located right beside the OOI HYPM mooring (de Jong et al., 2018). The resulting time series of CT, SA and σ_0 covers the period from 1 January 2002 to 31 December 2020. Because of our efforts to normalize the averaging of all data sets and all data sets are quality controlled for consistency with the other records before they are included, we assume that the uncertainty is uniform throughout the record. The Brunt-Väisälä frequency (N^2) was derived from the weekly SA and CT profiles using the TEOS-10 toolbox in order to determine the PV as $\mathrm{PV} = \frac{f}{g}N^2$.

We use mixed layer depth (MLD) as an indicator of local convection strength. The turbulent mixing during convection homogenizes the water column properties, thereby creating a mixed layer that is characterized by a nearly vertical profile of the hydrographic properties (CT, SA and σ_0). At the bottom of the mixed layer, the profile transitions to the stratified profile of the deeper water column not affected by mixing. However, because of the weak stratification at middepth (500–1,500 dbar) in the Irminger Sea throughout the year, it is difficult to determine the bottom of the mixed layer using density alone. This difficulty arises because there is nearly no observed density transition as the current year's mixed layer reaches previously convected water masses at this

21699291, 2025, 2, Downloaded from https://agupubs.onlinelibrary.wiley.com/doi/10.1029/2023JC020799, Wiley Online Library on [31/01/2025]. See the Terms and Conditions (https://onlinelibrary.wiley.com/terms-and-conditions) on Wiley Online Library for rules of use; OA articles are governed by the applicable Creative Commons License

Table 1
Overview of Number of Winter Profiles and Profiles With Mixed Layers

	Years covered	All profiles	Winter profiles	MLD > 200 dbar (after inspection)
LOCO mooring	2003–2018	4,969	1,918	283
OOI mooring	2014–2020	1,168	535	75
CIS mooring	2002–2016	4,769	1,966	273
Argo	2003–2020	969	264	57
Total		11,875	4,683	688

middepth. However, these new mixed layers do have temperature and salinity characteristics distinctive from water masses at middepth which can be used to determine accurate MLDs.

MLDs were determined separately for each individual profile of the LOCO, OOI, CIS moorings and for each Argo profile. An initial pass of the algorithm of Holte and Straneo (2017), which determines the MLD based on a straight line least squares fit (with an error tolerance of 1^−10) to temperature, salinity and density, provided a first separation into profiles with and without mixed layers. MLD from profiles starting below 200 dbar and profiles shorter than 500 dbar were discarded. Additionally, the mixed layer had to be at least 75 dbar thick. Of the remaining MLDs, it was required that the MLDs of temperature and salinity were within 50 dbar of each other and the MLD for density was similarly within 50 dbar or deeper. The shallowest of the three MLD is then used as MLD. Even with these requirements, the algorithm still selected MLDs that did not pass manual inspection; particularly for profiles that showed a transition that appeared like the bottom of a mixed layer but showed too much variability within the water column above the algorithm-determined MLD. These are likely remnants of recent mixed layers rather than active mixed layers. However, our interest here is in active mixing at the moorings. Since we cannot determine where these mixed layers were formed before they were advected to the moorings these MLDs were also removed. Out of a total of 4,683 profiles from the months in which mixed layers typically can occur (December through April), 688 profiles (15%) showed an active MLD deeper than 200 dbar that passed inspection (Table 1). Lastly, time series of MLDs from all platforms were spatiotemporally merged into one 3-day average MLD time series for the CIS.

2.2. Ocean and Atmospheric Buoyancy Time Series

We are interested in the roles of stratification versus surface forcing in the interannual variability of Irminger Sea convection. The surface buoyancy forcing ($B_{forcing}$) in J kg^{-1} resulting from atmospheric fluxes is defined as:

$$B_{forcing} = \frac{g\alpha}{\rho_0 c_p} Q - \beta g S_0 (E - P)$$

where α is the thermal expansion, c_p is the specific heat capacity, Q is the net atmospheric heat flux, β is the haline contraction of seawater, S_0 is the surface salinity, E is evaporation and P is precipitation. With the first term on the right representing atmospheric thermal forcing and the second term representing atmospheric freshwater forcing, the role of heat versus freshwater forcing will be investigated by evaluating the two right hand terms separately. To calculate $B_{forcing}$, net shortwave and net longwave radiation, sensible and latent heat fluxes (for Q), and total precipitation and evaporation (for E-P) fields from the ERA5 atmospheric reanalysis were downloaded from the Copernicus Climate Data Store (https://cds.climate.copernicus.eu/cdsapp#!/dataset/reanalysis-era5-single-levels?tab=overview).

Daily ERA5 fields were used for the 2002–2020 period and monthly fields were used for 1950–2020. Josey et al. (2019) compared ERA5 heat fluxes to those derived from the Irminger Sea OOI SUMO (Surface Flux Mooring) mooring measurements and found them to be consistent. Similarly, Renfrew et al. (2021) compared ERA5 to surface flux measurements north of Iceland and found them to compare well over the open ocean. At each time step, Q and E-P were averaged over our study region (the ellipse in Figure 1) as well as obtained directly from the grid point closest to the LOCO mooring location. The two time series are nearly identical, with correlations of 0.996 (for Q) and 0.97 (for E-P) and differences in the mean of 2% (for Q) and 5% (for E-P) with the

21699291, 2025, 2, Downloaded from https://agupubs.onlinelibrary.wiley.com/doi/10.1029/2023JC020799, Wiley Online Library on [31/01/2025]. See the Terms and Conditions (https://onlinelibrary.wiley.com/terms-and-conditions) on Wiley Online Library for rules of use; OA articles are governed by the applicable Creative Commons License

point values being higher than the area average. In the remainder of this manuscript we will use the fluxes averaged over the ellipse in Figure 1.

To quantify the stratification, we calculated the buoyancy of the water column between different depths from the mooring/Argo record as well as from the decadal hydrographic record. The water column buoyancy (B_{ocean}) in J kg^{-1} integrated over the layer between the upper boundary (z_{up}) and a reference level (z_{ref}) is defined as:

$$B_{ocean} = \frac{g}{\rho_0} \int_{z_{ref}}^{z_{up}} (\sigma_0(z) - \sigma_0(z_{ref}))\, dz$$

where g is the gravitational acceleration, $\sigma_0(z)$ is the potential density profile and ρ_0 is a fixed reference density (Bilo et al., 2022; Schmidt & Send, 2007). The advantage of this definition of stratification is that it has identical units to $B_{forcing}$, which facilitates a one-to-one comparison. The variability in the B_{ocean} time series over various layers compares well to that in N^2 and PV averaged over the same layers (Text S3 and Figure S3 in Supporting Information S1) giving us the confidence to use B_{ocean} as a measure of stratification.

2.3. Decadal Time Series From Shipboard Hydrography

To put the variability over the 19 years of the mooring record into longer term context, we extended the 1950–2009 multi-decadal time series of (near-)annual hydrography for temperature, salinity, and density in the CIS described by van Aken et al. (2011) to 2020. This time series includes historical data (from sample bottles) for the pre-World Ocean Circulation Experiment (WOCE) period from 1950 until 1989, and high-quality hydrographic data collected during near-annual repeat CTD surveys of the AR7 hydrographic section, the original survey line on which the location of the OSNAP array was based, from 1990 onwards (http://cchdo.ucsd.edu/). CTD data from 2014 onwards was mainly collected during the cruises that serviced the OOI and OSNAP moorings. The AR7 East (AR7E) hydrographic sections were surveyed predominantly in summer (April to October) to avoid ice conditions and the storm season. The time series therefore represents stratified summer conditions and does not capture seasonal changes or winter MLDs. However, it does capture the inter-annual through decadal changes in upper ocean stratification as well as changes in the low PV conditions at mid-depths resulting from strong winter convection (described in more detail in van Aken et al., 2011).

Figure 2 shows the 70-year record with the mooring period indicated at the end. At first glance, the hydrography of the mooring period (panels 2b though 2e) does not stand out as exceptional compared to the longer record. The density classes formed by convection during the mooring-Argo record are similar, although the thickness of these density layers (especially the 27.75–27.8 kg m^{-3} class) was larger in the 1990s. The mooring-Argo period is interesting to study the role of stratification because it includes both very strong stratification in the upper 500 m around 2005 and very low stratification in the same layer toward the end (panel 2a). This change in stratification was mainly temperature driven, with the early 2000s being warm and the late 2010s being colder. Changes in salinity had an opposite, but smaller, effect on stratification. The atmospheric forcing exhibits high interannual variability (panel 2a), but the 5-year running mean of the forcing shows that the mooring period was not exceptional. Since the variability in the hydrography and atmospheric forcing during the mooring period covers the range of the longer-term record, the climatology allowed by the higher temporal resolution data will also be representative of conditions in the Irminger Sea over the last 70 years. Similarly, because the last 19 years cover nearly the full range of stratification observed over the last 70 years, as well as periods of both weak and strong convection, our investigation of the respective influence of stratification versus forcing on convection strength is likely generalizable to the full 70-year record.

2.4. The PWP Mixed-Layer Model

We use a one-dimensional mixed-layer model to distinguish between the roles of atmospheric forcing and water-column stratification on the variability of winter convection in the Irminger Sea. The Price, Weller and Pinkel or PWP model (Price et al., 1986) has previously been used in the North Atlantic by Lazarevich et al. (2004). In that study, the authors demonstrated that the PWP model was capable of reproducing year-long float-observed sea surface temperatures to within 1°C, as well as the timing of the ventilation and stratification of the mixed layer.

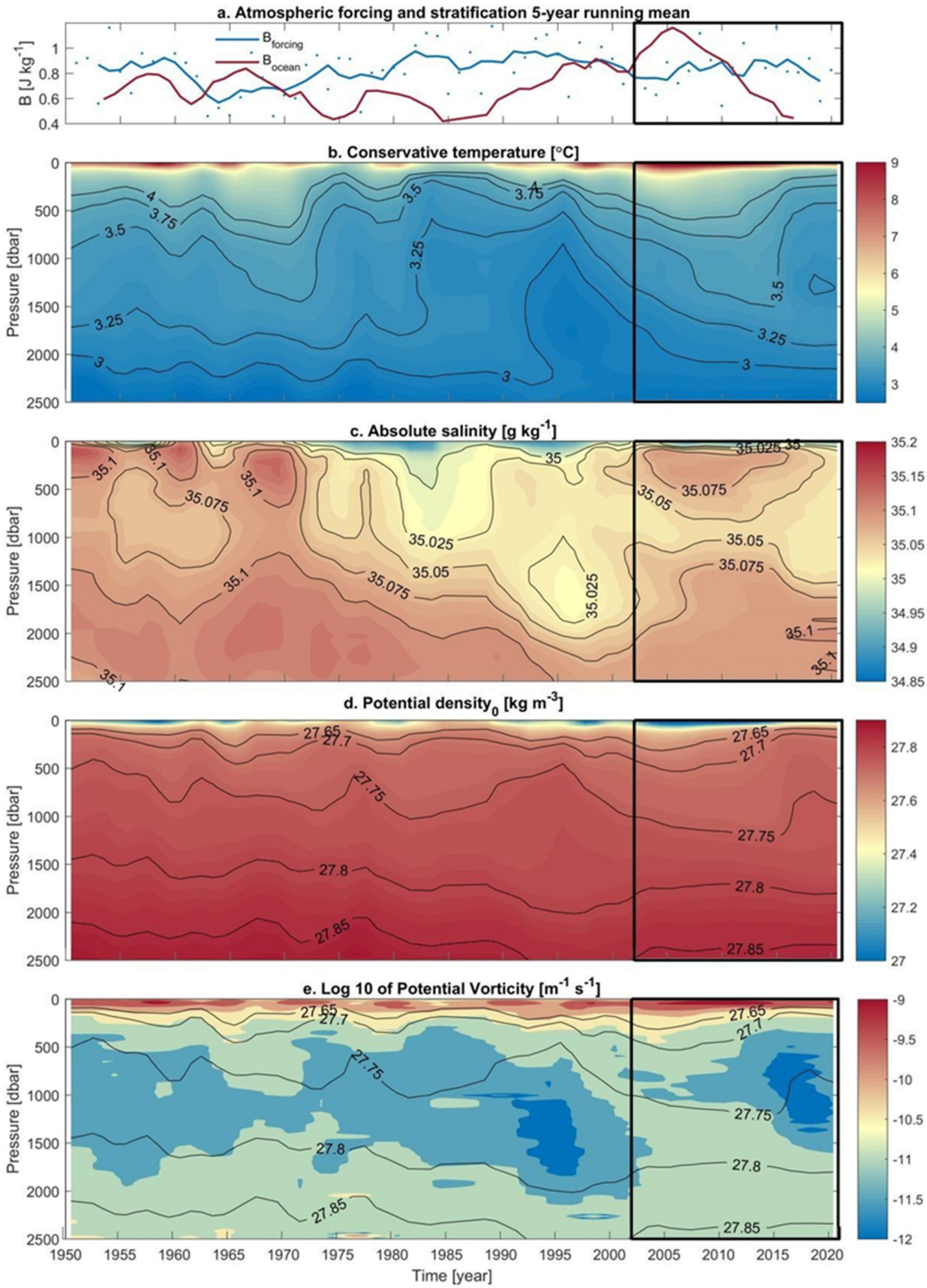

Figure 2. Central Irminger Sea multi-decadal hydrographic time series of (a) 5-year running mean values of the stratification over the upper 1,000 m (red) and the cumulative atmospheric forcing (blue). Annual forcing values shown as blue dots. (b) conservative temperature, (c) absolute salinity, (d) potential density, and (e) potential vorticity. The mooring period is indicated with the black box.

21699291, 2025, 2, Downloaded from https://agupubs.onlinelibrary.wiley.com/doi/10.1029/2023JC020799, Wiley Online Library on [31/01/2025]. See the Terms and Conditions (https://onlinelibrary.wiley.com/terms-and-conditions) on Wiley Online Library for rules of use; OA articles are governed by the applicable Creative Commons License

21699291, 2025, 2, Downloaded from https://agupubs.onlinelibrary.wiley.com/doi/10.1029/2023JC020799, Wiley Online Library on [31/01/2025]. See the Terms and Conditions (https://onlinelibrary.wiley.com/terms-and-conditions) on Wiley Online Library for rules of use; OA articles are governed by the applicable Creative Commons License

Briefly, the PWP model is a vertical, bulk mixed-layer model that simulates the evolution of water-column temperature and salinity as a result of atmospheric forcing. The model requires an initial temperature and salinity profile and inputs of surface heat, freshwater and momentum fluxes. Precipitation, long-wave radiation, sensible heat, and latent heat are input at the ocean surface. Incoming shortwave radiation was modeled as a function of depth according to Paulson and Simpson (1977) using the optical properties of a 1b water type (Jerlov, 1968). Static instability in the density profile of the mixed layer is removed by entraining water from below until stability is achieved. Bulk and gradient Richardson numbers are determined, and if found below critical thresholds (bulk <0.65 and gradient <0.25), deeper water is entrained and the process is repeated until vertical stability is achieved (Price et al., 1986). The result is a bulk mixed layer in which all properties (e.g., temperature, salinity, chemical species) are uniformly distributed. See Price et al. (1986) for more details.

In this study, PWP model experiments were performed for the Irminger Sea, each with different initializing water-column conditions and surface forcing records. On September 1 of each year, model runs were initialized using the mean SA and CT profiles collected during the period of maximum water-column stratification, occurring in the Irminger Sea from mid-August to mid-September. PWP experiments were forced with inputs of surface heat, freshwater and momentum fluxes from ERA5 Reanalysis products for the Irminger Sea (60°N, 39.5°W; Hersbach et al., 2018). ERA5 Reanalysis products for 6-hr intervals were interpolated to 1-hr intervals and used to force the model for a year. At each time step, profiles of temperature, salinity, and momentum were determined, with model outputs of MLD and water-column temperature, salinity and density being saved every 3.5 days. Density was calculated using the full equation of state. Three types of PWP experiments were performed:

Experiment type 1: Yearly reconstruction of the observed MLD variability from 2003 to 2020. Each year, the PWP model is initialized with the observed maximum-stratification water-column profiles of that particular year and forced with the corresponding year-long surface fluxes.

Experiment type 2: Role of varying water-column stratification in interannual MLD variability.

PWP model runs are initialized each year with the observed maximum-stratification water-column profiles from that year. Surface forcing is not varied, rather the surface fluxes of one winter are used to force all winters.

Experiment type 3: Role of varying surface forcing in interannual MLD variability. The stratification is not varied, the PWP model runs are initialized with the same water-column profiles each year, but forced with the unique surface fluxes of the particular year.

Multiple versions of experiment type 2 (using various example winters) and type 3 (using various example stratifications) have been done. In total, 137 years-long PWP runs spanning the full range of stratification and forcing conditions were done.

3. Description of Irminger Sea Convection: Climatology and Interannual Variability

The data sets presented above provide an unique opportunity to describe convection in the CIS, to study its variability over interannual and decadal time scales, and to investigate the respective driving forces of variability. The mooring record documents several periods of weak convection (MLD < 500 m) as well as several periods of strong (MLD > 1,000 m) convection (described in more detail in Section 3.2).

3.1. Climatology of 2002–2020 Irminger Sea Convection

In Figure 3, we present seasonal climatologies for the surface buoyancy forcing, MLD, Absolute Dynamic Topography (ADT) and the mixed-layer temperature, salinity and density. ADT was retrieved from the ARMOR 3D 0.25° data set at Copernicus (Mulet et al., 2012). Both the monthly mean climatological values with standard deviations, as well as the daily means for each day of the year are shown. Additionally, we show the daily climatology of the SST, salinity in the upper 50 m (Argo, OOI surface mooring), and derived density over the same time period. Note that all the shallow (<100 m) MLDs in summer are from Argo profiles as these cannot be determined from the subsurface mooring profilers.

The seasonal climatology shows that heat fluxes largely determine the total buoyancy lost to the atmosphere in winter (Figure 3a). The Irminger Sea gains buoyancy through freshwater year round, but the atmospheric freshwater fluxes are an order of magnitude smaller and fairly constant throughout the year. The large standard deviations in winter, mainly seen in the heat and total fluxes, indicate both intermittency in heat fluxes (short

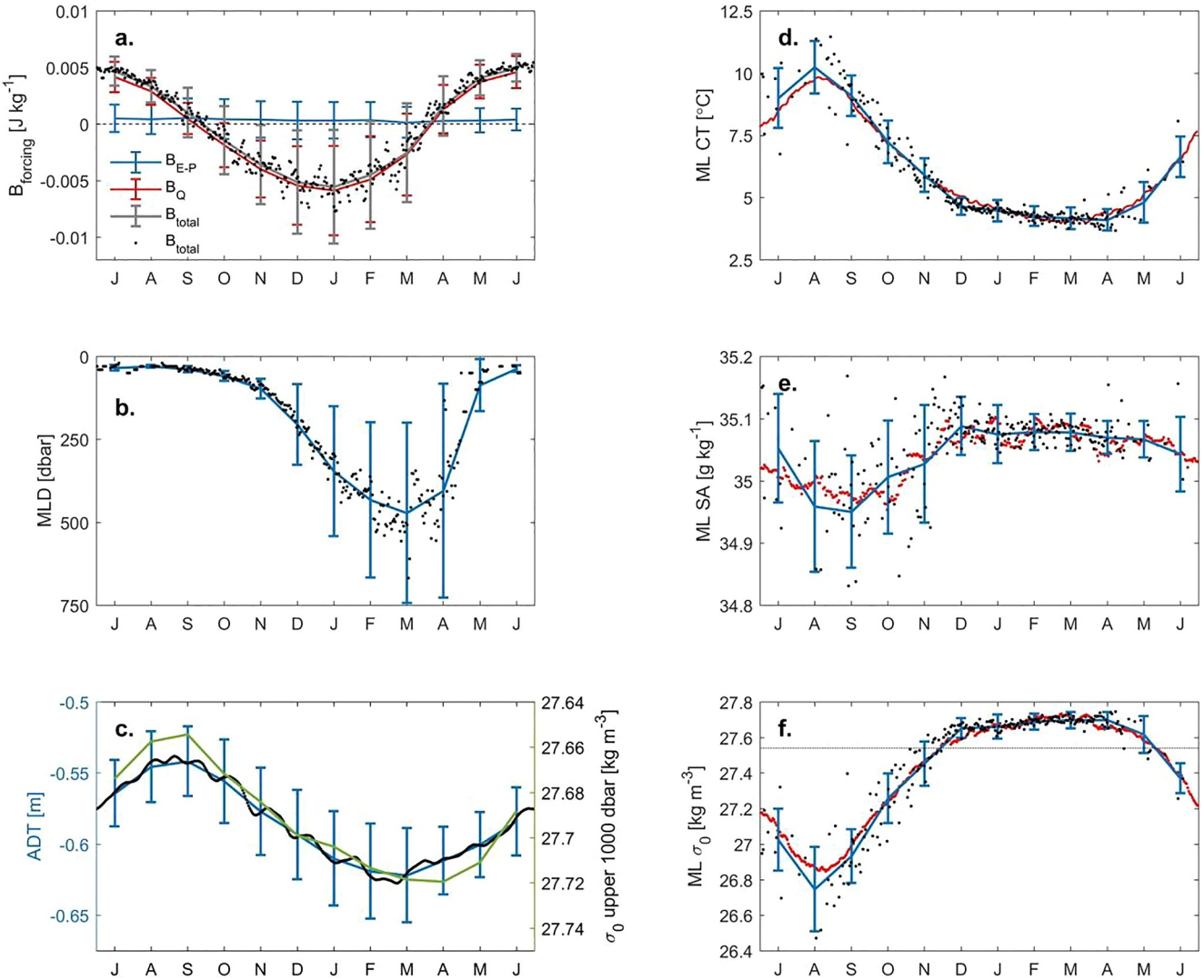

Figure 3. Seasonal climatologies of properties associated with convection in the central Irminger Sea. A start date of 1 July was chosen to show evolution of MLDs through a complete winter. Black points in each of the panels indicate daily means with the lines and error bars representing the monthly mean and standard deviation. (a) Seasonal climatology of surface buoyancy forcing (J/kg). Plotted are the components derived from heat fluxes (B_Q in red), freshwater fluxes (B_{E-P} in blue) and the total atmospheric buoyancy flux (B_{total} in gray and black). Zero line is dashed. (b) Mixed layer depth (MLD, dbar). (c) Absolute dynamic topography (ADT, m in blue and black) and mean potential density over the upper 1,000 dbar of the water column (σ_0, kg m^{-3} in green). (d) Mixed layer conservative temperature (CT) (ML CT °C in blue and black) and sea surface temperature (SST) (in red). (e) Mixed layer absolute salinity (ML SA, g kg^{-1} in blue and black) and daily upper 50 m absolute salinity (in red). (f) Mixed layer potential density (ML σ_0, kg m^{-3} in blue and black) and potential density calculated from SST and 50 m salinity (in red). The gray line is the potential density of the maximum overturning for Overturning in the Subpolar North Atlantic Program East (27.54 kg m^{-3}).

lasting high flux events alternating with calm days) and interannual variability (discussed in more detail in Section 3.2). Heat fluxes add buoyancy from April through September, but remove more buoyancy from October to March through stronger heat fluxes, thus leading to a net loss of heat and buoyancy over the year.

Even though the Irminger Sea gains buoyancy over summers, it is a relatively windy region year round (Duyck et al., 2022). Therefore shallow mixed layers are common throughout summer (Figure 3b). The atmospheric freshwater forcing (net gain) is collected in this upper layer (Sterl & de Jong, 2022) creating a minimum salinity around September. This thin fresh layer warms through spring and summer (Figures 3a and 3d), reaching its highest temperature (Figure 3d) and lowest density in August (Figure 3f). In September, the ocean starts to lose heat to the atmosphere and the surface and ML temperature decreases quickly. Through October and November, the surface heat fluxes increase further, but are mainly still removing heat from the upper 100 dbar. With most of the heat removed from this upper layer, and strong heat loss occurring from December to March, the

21699291, 2025, 2, Downloaded from https://agupubs.onlinelibrary.wiley.com/doi/10.1029/2023JC020799, Wiley Online Library on [31/01/2025]. See the Terms and Conditions (https://onlinelibrary.wiley.com/terms-and-conditions) on Wiley Online Library for rules of use; OA articles are governed by the applicable Creative Commons License

21699291, 2025, 2, Downloaded from https://agupubs.onlinelibrary.wiley.com/doi/10.1029/2023JC020799, Wiley Online Library on [31/01/2025]. See the Terms and Conditions (https://onlinelibrary.wiley.com/terms-and-conditions) on Wiley Online Library for rules of use; OA articles are governed by the applicable Creative Commons License

climatological MLD gradually deepens from 205 ± 122 dbar in December to 471 ± 271 dbar in March. Generally, heat loss weakens in April, leading to a sudden shallowing of the MLD. However, in strong winters that occasionally last through April, the MLD deepens further leading to a bigger standard deviation for April (405 ± 322 dbar) compared to March. In May, the heat fluxes change sign and the ocean gains heat causing a sudden halt to convection. SST starts to increase and MLDs shallow to 87 ± 79 dbar.

The hydrographic climatologies show that the density follows the changes in temperature. Temperature decreases steeply from a climatological maximum of 10.2 ± 1.0°C in August to 4.6 ± 0.3°C in December and then gradually decreasing further to a minimum of 4.1 ± 0.4°C in April. The gradual decline during strong surface fluxes is due to the heat loss being spread over a thicker mixed layer. Sea surface temperature from ERA5 follows the mixed layer temperature closely. The potential density changes from an August minimum density of 26.75 ± 0.24 kg m^{-3} to 27.65 ± 0.06 kg m^{-3} in December and then increasing gradually to a maximum in March and April of 27.70 ± 0.05 kg m^{-3}. Salinity decreases through summer, due to accumulating freshwater from precipitation and possibly a freshwater export from Greenland. In September the climatological salinity is 34.95 ± 0.09 g kg^{-1}. The large standard deviation reflects large differences between different summers, as some were characterized by significantly fresher anomalies (Bilo et al., 2021; Oltmanns et al., 2018; Sterl & de Jong, 2022). Salinity increases as the mixed layer deepens below this fresh summer layer and reaches into the more saline Subpolar Mode Water (SPMW) underneath. However, there is a second inversion in the vertical salinity profile, with fresher waters at mid-depths (locally convective water from previous winters and Labrador Sea Water (LSW)). Thus, as mixed layers deepen beneath the SPMW into this fresher layer from December onwards the salinity gradually decreases.

Overall, the standard deviations of the hydrographic properties decrease as the MLD deepens. This is also seen in records of instruments at fixed depths with higher temporal resolution (de Jong et al., 2018). It reflects the (nearly) absent gradients within the mixed layer, the changes in heat and freshwater applied at the surface being spread over a thicker layer, as well as the fact that this takes place over a substantial area, thus reducing lateral gradients. This vertical and lateral homogenization ceases as winter cooling ends and restratification sets in, leaving behind the characteristic homogeneous convective water mass at mid-depths with a typical low PV signature.

Sea surface height, or ADT, is largely a function of steric height and will be affected by density changes over a large part of the water column. This is confirmed by the seasonal cycle of ADT that follows that of the density of the upper 1,000 dbar of the water column. However, the timing of the minima is offset by 1 month, with ADT increasing slightly before density does. This offset disappears if a layer of 250 dbar or shallower is used for the mean density (not shown), indicating that the onset of restratification of this upper layer causes the increase of ADT.

3.2. Interannual Variability During the 2002–2020 Period

There is large interannual variability in MLD in the CIS (de Jong et al., 2012), resulting in large standard deviations in the monthly climatology (Figure 3). Here we investigate the interannual variability further using the 19-year mooring-Argo record. Figure 4 shows the merged mooring-Argo records of temperature, salinity, density, and PV with MLD, with the latter two giving the most insight into the strength of convection in each winter. We will denote winters by the last digits of the years in which they occur, for example, the winter of 2002–2003 as 02–03.

At the start of the record in 2002, the water column was relatively fresh and a weak PV minimum can be seen around 700 to 1,000 dbar. The first five winters (the winters of 02–03 to 06–07) did not see intense convection, with MLDs between 395 and 620 dbar. This layer restratifies fully in summer (Sterl & de Jong, 2022), and therefore these MLD did not make an imprint of low PV on the water column that remained after winter. During this period, the water column warmed and became more saline, continuing the ongoing restratification of the Irminger Basin after the intense convection in the 1990s (van Aken et al., 2011). The winters of 07–08 and 08–09 were the first winters in the mooring record where convective mixing reached just below 800 dbar and a low PV signature remained visible at these mid-depths. The next winter (09–10) had the shallowest convective mixing observed in the record, a MLD of a mere 288 dbar, and was followed by another winter with fairly weak convection (500 dbar in 10–11). A winter with intense convection (998 dbar) followed in 2011–2012. Interestingly, during the next two winters (12–13 and 13–14) convection was weak (MLD of 572 and 650 dbar respectively), but an imprint can be seen in PV. This suggests that deeper mixing may have occurred nearby, after which low PV water was advected to the mooring location. Both the winters of 14–15 and 15–16 showed the strongest convection of the record, with MLD of 1,500 and 1,250 dbar, respectively. Convection remained strong through 16–17 and 17–18, with MLD of 880 and 1,020 dbar. In the last two winters of this record, 18–19 and 19–20,

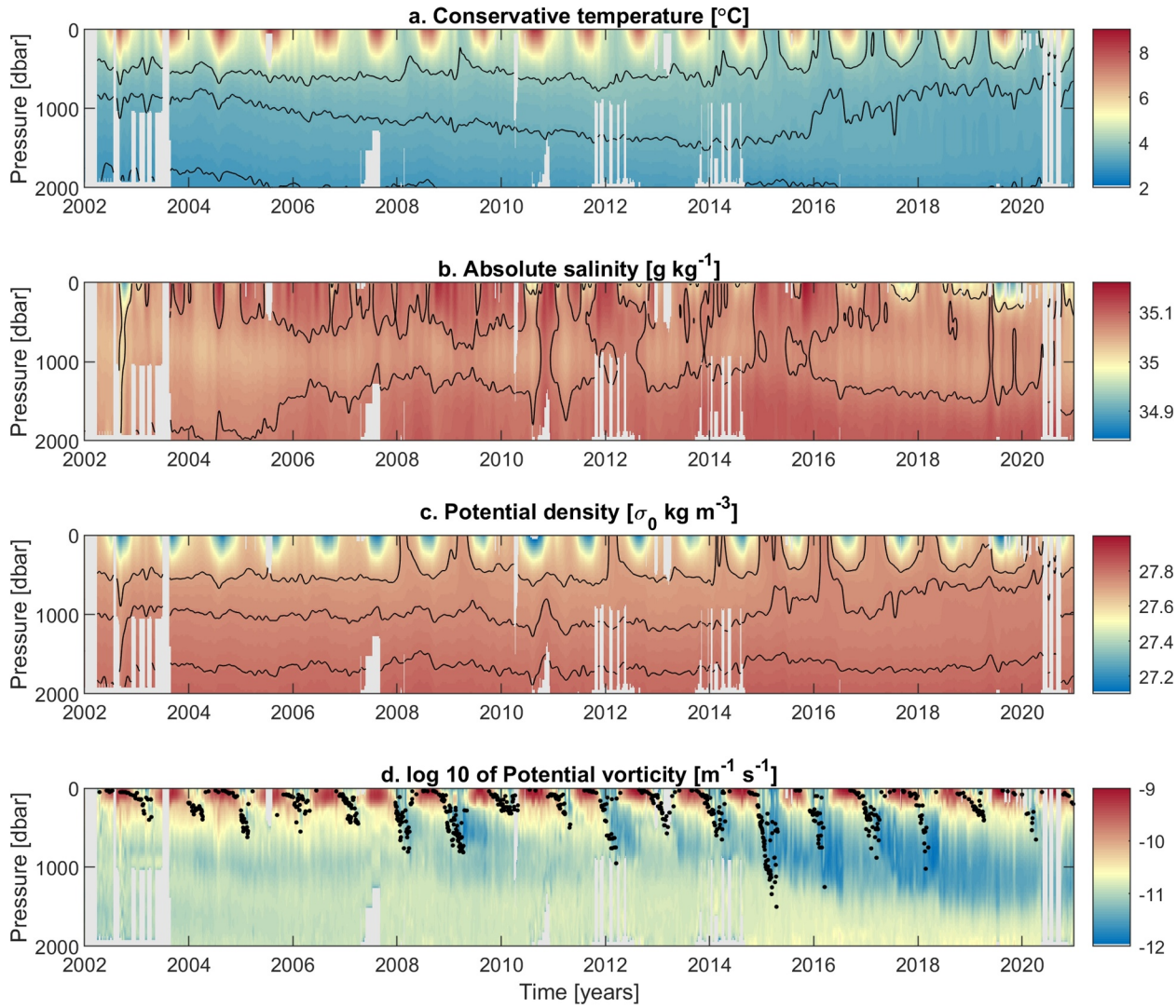

Figure 4. Weekly merged 25-dbar mooring and Argo data product from 2002 to 2020. (a) Conservative temperature with black contours at 3, 3.5 and 4°C, (b) Absolute salinity with black contours at 35.025 and 35.075 g kg^{-1}, (c) Potential density (color), with black contours at 27.7, 27.75 and 27.8 kg m^{-3}, and (d) Potential vorticity (in color) and mixed layer depth (black dots).

convection was weak (408 and 650 dbar). The occurrence of intense convection during four consecutive winters (14–15 through 17–18), freshened the upper 1,200 m of the water column. The local freshening was further aided by the arrival of a fresh anomaly in the near surface layer seen in the upper 100 dbar in Figure 4b. This anomaly is also described by de Jong et al. (2020); Holliday et al. (2020); and Biló et al. (2022). It reversed the trend of warming and salinification in the CIS. This has resulted in the intermediate waters (750–1,500 m) becoming colder and fresher (Figure 4b). Despite the lower salinities, the cold character of the strong convection from 2014 to 2018 created a dense class of intermediate waters in the Irminger Sea with a low PV signature of convection that remains visible after the weaker convection of the last two winters (Figure 4d).

The impact of the interannual variability in convection on the density in the upper 1,000 dbar of the water column, and thereby on ADT is clear from Figure 5. The density averaged over the upper 1,000 dbar for the whole period exhibits a strong seasonal cycle. Winter mixed layers set the maximum density each year and restratification decreases density through spring and summer. The ADT time series closely follows that of the upper 1,000 dbar density.

Winters with deeper MLD create denser convective waters (Figure 6c), which depresses the height of the sea surface further. The winters of 07–08 and 11–12 particularly showed steeper drops in ADT compared to the

21699291, 2025, 2, Downloaded from https://agupubs.onlinelibrary.wiley.com/doi/10.1029/2023JC020799, Wiley Online Library on [31/01/2025]. See the Terms and Conditions (https://onlinelibrary.wiley.com/terms-and-conditions) on Wiley Online Library for rules of use; OA articles are governed by the applicable Creative Commons License

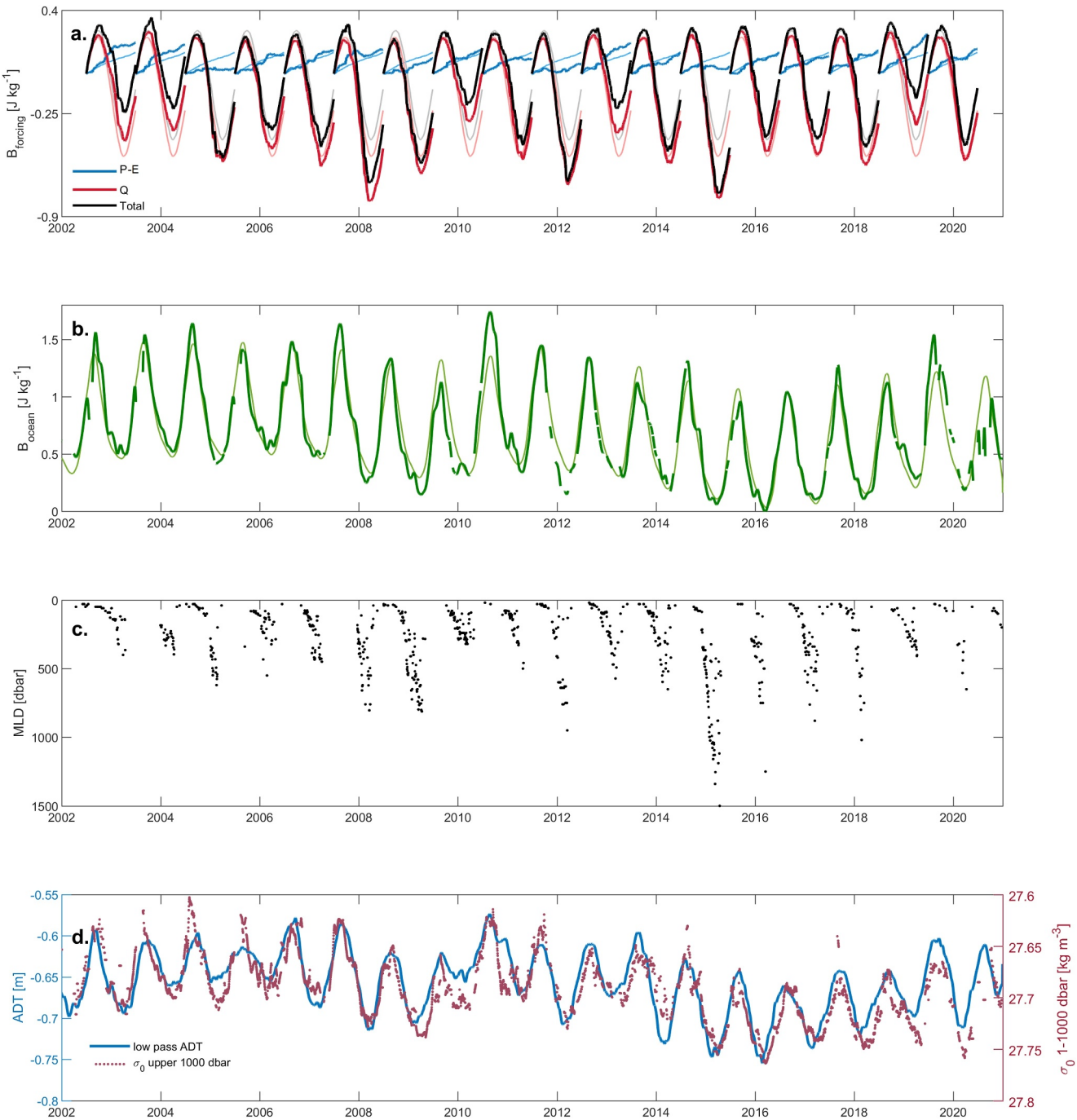

Figure 5. Cumulative surface buoyancy forcing starting at 1 July of each year, water column buoyancy, mixed layer depth (MLD), upper 1,000 dbar density and Absolute Dynamic Topography (ADT). (a) shows the total cumulative buoyancy forcing (thick black line) as well as the contribution of heat fluxes (Q, thick red line) and freshwater fluxes (P-E, thick blue line) to the total flux. Thinner lines of corresponding colors represent the seasonal climatology. (b) Water column buoyancy integrated between 1,000 dbar and the surface (thick green line). Thin light green line is the seasonal climatology super positioned on the low pass (3-year running mean) time series, highlighting years with stronger than average break down or build up of stratification. (c) MLD. (d) Density averaged over the upper 1,000 dbar of the water column (red dots), low-pass filtered (30-day running mean) ADT (m, thick blue line).

previous winter. Both the seasonal cycle and the interannual variability cause a strong correlation between ADT and density. The maximum correlations are found at the surface, with a correlation of −0.83 between 30-day low-passed σ_0 and ADT. After deseasoning these time series, by removing daily climatology, the correlation is −0.68. These correlations decrease approximately linearly with depth until they are about zero at 1,200 dbar depth. Thus,

21699291, 2025, 2, Downloaded from https://agupubs.onlinelibrary.wiley.com/doi/10.1029/2023JC020799, Wiley Online Library on [31/01/2025]. See the Terms and Conditions (https://onlinelibrary.wiley.com/terms-and-conditions) on Wiley Online Library for rules of use; OA articles are governed by the applicable Creative Commons License

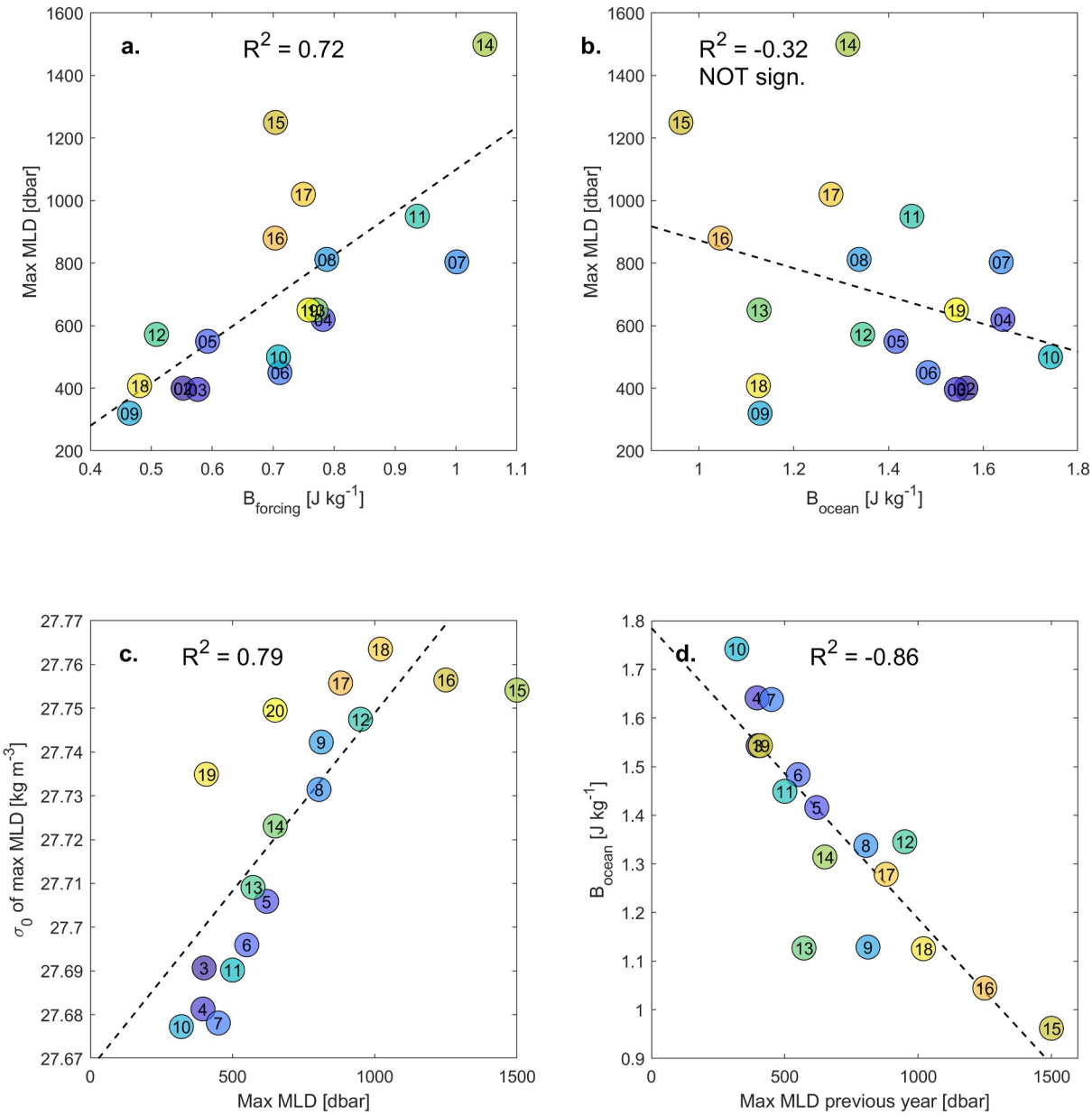

Figure 6. Scatter plots of interannual variability. (a) Annual maximum mixed layer depth (MLD) against maximum cumulative surface buoyancy ($B_{forcing}$) loss over winter (fall maximum—spring minimum in Figure 5), (b) Annual maximum MLD against annual maximum water column buoyancy (B_{ocean}) over the upper 1,000 dbar in the summer preceding these MLDs, (c) Annual maximum ML density against annual maximum MLD. (d) Annual maximum water column buoyancy (B_{ocean}) over upper 1,000 dbar against maximum MLD in the preceding winter. The color of the markers shows the progression through the record, and the last digits of the year are also indicated in the marker. Correlations, and whether they pass a 95% significance test, are also indicated.

the interannual variations in ADT are linked with the variability in the upper part of the water column, which is associated with local convection and restratification. The lack of correlation at the depth of LSW indicates that waters advected from the Labrador Sea do not contribute significantly to the variability of σ_0 and ADT in the CIS. Thus, ADT may be used as a proxy of local upper water column density.

4. Attribution of Variability: Ocean Stratification Versus Atmospheric Forcing

4.1. Stratification Versus Forcing in the Mooring-Argo Time Series

There is ongoing discussion concerning the relative roles of the surface buoyancy forcing versus the water column stratification in determining the MLD in the Irminger Sea (Bilo et al., 2022). Figure 5 shows the interannual

21699291, 2025, 2, Downloaded from https://agupubs.onlinelibrary.wiley.com/doi/10.1029/2023JC020799, Wiley Online Library on [31/01/2025]. See the Terms and Conditions (https://onlinelibrary.wiley.com/terms-and-conditions) on Wiley Online Library for rules of use; OA articles are governed by the applicable Creative Commons License

21699291, 2025, 2, Downloaded from https://agupubs.onlinelibrary.wiley.com/doi/10.1029/2023JC020799, Wiley Online Library on [31/01/2025]. See the Terms and Conditions (https://onlinelibrary.wiley.com/terms-and-conditions) on Wiley Online Library for rules of use; OA articles are governed by the applicable Creative Commons License

variability of the cumulative heat, freshwater and total buoyancy forcing over each winter, as well as the time series of water-column stratification of the upper 1,000 dbar. Even though there is considerable variability in freshwater fluxes (Figure 5a), the variability in heat fluxes dominates the interannual variability of the total buoyancy loss in winter. The strongest winters in this 2002-2020 record are the winters of 07–08, 11–12 and 14–15. All these winters showed a deepening of the MLD with respect to previous years. There are a number of years with weak surface buoyancy forcing, particularly 03–04, 09–10, 12–13 and 18–19. These are also the years with the shallowest MLD (Figure 5c) and relatively small winter drops in ADT (Figure 5d).

Notably, the water-column buoyancy shows a seasonal cycle that is dominant over interannual variability (Figure 5b). This seasonal cycle is mainly contained in the upper 500 dbar of the water column, while waters below mainly show interannual variability (Figure S2 in Supporting Information S1). We here integrate B_{ocean} over the upper 1,000 dbar of the water column. This contains both the contribution to this seasonal cycle that comes from the upper 500 dbar of the water column and the interannual signal in the layer between 500 and 1,000 dbar that is derived from local convection. During periods of strong convection (MLD ≥800 dbar) the buoyancy of the layer between 500 and 1,000 dbar is reduced and minima of B_{ocean} reached in winter are lower. In most years, the summer maximum of B_{ocean} is nearly indistinguishable from what would be expected from the climatology (thin line Figure 5b), indicating that the interannual variability in the restratification of the water-column buoyancy is small. Only a few years stand out as having a stronger stratification built up through summer. These are the summers of 2007, 2010 and 2019. The strengthening of stratification in these years is (at least partly) the result of larger than average atmospheric freshwater fluxes (Figure 5a) leading to an anomalously fresh and warm near surface layer. However, over most of the profile above 1,200 m, temperature is the dominant driver of density changes (further explained in Supporting Information S1). A more thorough description of restratification in the Irminger Sea can be found in Sterl and de Jong (2022).

By distilling the data in Figure 5 to annual extremes, we get a first insight into the relative importance of interannual variability in atmospheric forcing ($B_{forcing}$) versus stratification (B_{ocean}) to the MLD and the properties of the CIS (Figure 6). As expected, there is a strong correlation (Figure 6a) between the total accumulated heat loss through winter and the annual maximum MLD in that winter. However, there is only a very weak and not statistically significant correlation (Figure 6b) between annual maximum summer stratification and the annual maximum MLD in the following winter. Thus, the MLD is solely determined by the forcing and not by the stratification before winter. Deeper MLDs result in a higher mixed layer density (Figure 6c), with a progression from lighter and shallower mixed layers at the start of the record to deeper and denser mixed layers at the end. Due to vertical mixing and increase in density of the upper water column by convection, there is a very strong relation between the maximum MLD in winter and the maximum stratification in the following summer (Figure 6d). So, the stratification in the Irminger Sea is dependent on the MLD in the preceding winter, but the MLD is not dependent on the stratification in its preceding summer. This finding is aligned with Sterl and de Jong (2022), who determined from reanalysis data that the restratification over the upper 600 m is fairly constant from year to year and mainly depends on the convection in the preceding winter.

4.2. Stratification Versus Forcing in the PWP Model

Three types of experiments were done with the PWP model to further test the sensitivity of the MLD to the atmospheric buoyancy forcing and the initial water-column buoyancy. The first type of experiment, which aimed to reproduce the variability in MLD observed in the mooring-Argo record, was simulated by applying the unique surface forcing of each winter to a water column initialized with the observed temperature and salinity profiles at the time of maximum water-column stratification of the preceding summer. PWP outputs of MLD every 3.5 days are compared with observations, and overall, the reproduced interannual variability in MLD matches the observed MLD well, with a root mean square error (RMSE) of 253 and correlation of 0.76 (Figure 7a) although it tends to overestimate MLD in some years (especially 2010) and underestimates in 2006 and 2015.

The second type of PWP experiment aimed to show the role of variable surface forcing on MLD by applying different surface forcing to the same initializing set of temperature and salinity profiles. By using identical initialization profiles for each year in this type of experiments, the interannual variability in the atmospheric forcing is maintained and the influence of varying stratification is removed. In the example shown in Figure 7b, the unique surface forcing of each year was applied to the mean initializing profile, calculated as the mean of all maximum water-column stratification temperature and salinity profiles. Somewhat surprisingly, PWP MLD

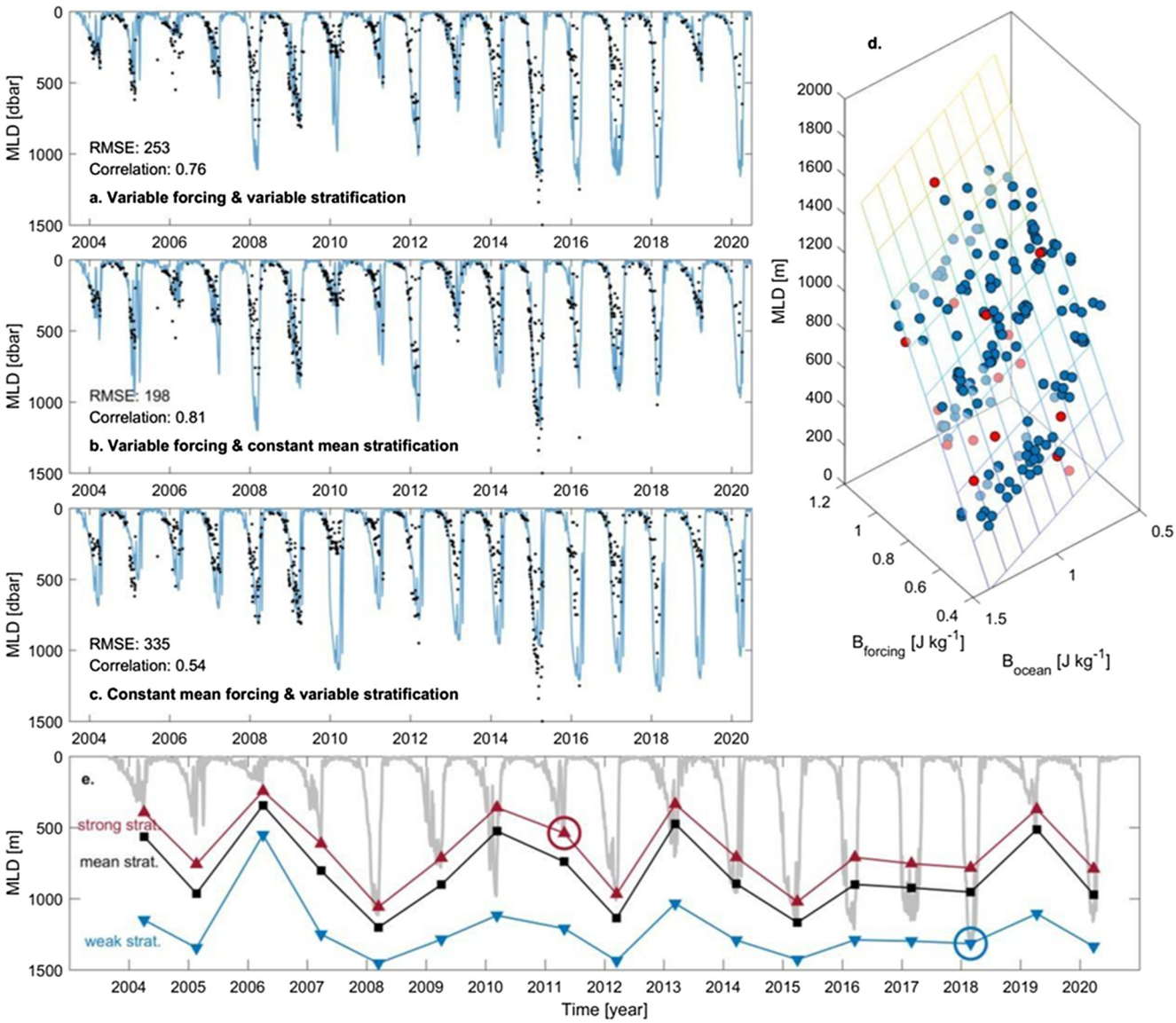

Figure 7. Results from the PWP experiments. Panels (a–c) show mixed layer depth (MLD) outputs from an example of each of the three types of PWP model experiments (in blue) compared to observed MLD (in black). (a). Reconstruction of observed variability in MLD with both varying forcing and stratification, (b) investigating role of forcing by applying the observed variable forcing and initializing using summer mean constant stratification, (c) investigating the role of stratification by applying the identical forcing each year and re-initializing annually with the observed summer stratification. The root mean square error and the correlation (significant at the 95% level) between modeled and observed MLD is noted in each panel. (d) grided surface shows the 2-D linear regression fit of annual maximum MLD on $B_{forcing}$ and B_{ocean} over the upper 1,000 m. PWP points used for fit are shown in blue, observations in red. Lighter shading indicates data points behind the 2-D linear regression fit. (e) Annual maximum PWP MLD under different stratifications. Observed forcing is applied to the same initializing water-column profiles representing strong (2010 summer condition, in red), average (in black), or weak (2017 summer conditions, in blue) water-column stratification. Model MLD outputs using variable forcing and water-column initializations (Experiment 1, panel a) are shown in gray.

outputs using record-average initializing profiles and unique surface forcings match the observed MLD slightly better (possibly not significantly so) with a slightly higher correlation of 0.81 and a lower RMSE of 198 than the first type of experiment using both the observed stratification and the observed forcing (Figure 7b, as compared to Figure 7a). This indicates minimal or no loss of model fidelity in reproducing the observed MLD record when the influence of inter annually varying stratification is removed. In particular, using the mean stratification reduced the MLD simulated for 09–10, and 15–16 through 17–18, which were overestimated in Figure 7a.

21699291, 2025, 2, Downloaded from https://agupubs.onlinelibrary.wiley.com/doi/10.1029/2023JC020799, Wiley Online Library on [31/01/2025]. See the Terms and Conditions (https://onlinelibrary.wiley.com/terms-and-conditions) on Wiley Online Library for rules of use; OA articles are governed by the applicable Creative Commons License

21699291, 2025, 2, Downloaded from https://agupubs.onlinelibrary.wiley.com/doi/10.1029/2023JC020799, Wiley Online Library on [31/01/2025]. See the Terms and Conditions (https://onlinelibrary.wiley.com/terms-and-conditions) on Wiley Online Library for rules of use; OA articles are governed by the applicable Creative Commons License

The third type of experiment aimed to show the role of varying water-column stratification on MLDs. The model was initialized each year using the temperature and salinity profiles observed during maximum stratification from that summer, but forced with an identical surface forcing record. Different forcing records were chosen to represent average (12–13 and 15–16), weak (08–09 and 17–18) and strong (06–07 and 13–14) forcing years. In the example shown in Figure 7c, observed initialization profiles are forced using the 12–13 years. The 12–13 years was chosen as a normal year as its cumulative surface forcing of 0.73 J kg^{-1} was close to the 2002–2020 mean cumulative surface forcing (Mean $B_{forcing}$ = 0.71 J kg^{-1}). We chose to use a representative individual winter's forcing for this experiment type rather than a smooth climatological mean in order to maintain some of the intermittency of heat fluxes within a winter. However, since the total applied atmospheric forcing is the same it should not affect the maximum reached MLD. Notably, this constant forcing experiment performs worse than the other two experiments, with a much lower correlation of 0.54 and higher RMSE of 335,mainly due to more frequent overestimations of MLDs.

It is interesting to also look at particular years. Notably, 2010 and 2019 stand out. The MLDs of these 2 years are simulated well in the variable forcing-variable stratification and the variable forcing-constant stratification experiments, but are highly (or deeply) overestimated in the constant forcing-variable stratification experiment. These 2 years are known for their exceptionally strong stratification, which has been suggested to be the cause of the shallow convection in these winters. However, from these results it becomes apparent that it is crucial to get the forcing of these 2 years correct in order to get the correct MLD.

The different PWP experiments enable us to look at the dependence of MLD on forcing and water-column buoyancy for more scenarios than the observation record allows. Figure 7d shows annual maximum MLDs against total winter forcing and pre-winter maximum water-column buoyancy for all observations (n = 17, in red) and PWP runs (n = 137, in blue). These 137 runs cover the full range of combinations of strength of B_{ocean} and $B_{forcing}$. Using only the PWP outputs, a multivariate (2D) linear regression of annual maximum MLD on total winter $B_{forcing}$ and pre-winter maximum B_{ocean} yields a dependence on $B_{forcing}$ that is about three times as large as that of B_{ocean}. The relation found using B_{ocean} over the upper 1,000 m and ERA5 for atmospheric forcing is $maxMLD = 1{,}775 \cdot B_{forcing} - 512 \cdot B_{ocean}$ with a significant correlation of 0.78 with the simulated MLDs. While this linear approximation is very simplified, based on a model taking only stratification and atmospheric forcing into account, it does fit the observations (in red in Figure 7d, these are not used for the fit) well as well.

While we find that the role of forcing is stronger in determining MLD, the impact of stratification under a series of different forcing scenarios is extremely important in the context of climate change trends and the projected increase in stratification in the future. We quantify the effect of stratification on MLD by running the PWP Experiment 2 initialized with a weakly versus average or strongly stratified water column and subjected to the observed 19 different atmospheric forcings (Figure 7e). Profiles from summer 2017 and 2010 are used to represent the weakest (B_{ocean} = 0.60 J kg^{-1}) and strongest stratification case (B_{ocean} = 1.04 J kg^{-1}), respectively. The average stratification case (B_{ocean} = 0.81 J kg^{-1}) is determined as the mean of temperature and salinity profiles during maximum water-column stratifications over the record, and is within 1% of the average between the weakest and strongest case. The mean MLD over all years in the weakly stratified case is 1,230 ± 211 m, versus 823 ± 257 m in the average stratification case and 655 ± 248 m in the strong stratification case. Thus, the mean deepening of 407 ± 121 m as a result of weak stratification is stronger than the mean shallowing of 170 ± 27 m as a result of stronger stratification.

Further examining the strong stratification case of 2010, the additional stratification was the result of a shallow (~60 m) warm and fresh layer. Once this layer is removed, the profile is very similar to other years. This results in the fairly constant shallow bias of 170 m in maximum MLD between the strong and average stratification cases. Notably, MLDs of 1,200 are still reached in the strong stratification case during years with strong forcing. The difference between MLD is larger and more variable between the weak and average stratification cases than the strong and average cases. The maximum MLD reached in the case of weak stratification is around 1,500 m and happens during multiple years. Even in years with strong forcing, the mixed layer does not deepen further. We suspect the density gradient between the convective waters and the overflow waters beneath contribute as a limiting factor to MLD here.

21699291, 2025, 2, Downloaded from https://agupubs.onlinelibrary.wiley.com/doi/10.1029/2023JC020799, Wiley Online Library on [31/01/2025]. See the Terms and Conditions (https://onlinelibrary.wiley.com/terms-and-conditions) on Wiley Online Library for rules of use; OA articles are governed by the applicable Creative Commons License

5. Discussion and Conclusions

We have presented here a novel weekly 19-year time series of hydrography and convection in the CIS (Figure 4) based on mooring and Argo float data collected from 2002 to 2020. Using a 70-year annual time series of shipboard hydrographic surveys (Figure 2), we have demonstrated that the variability in the hydrography, stratification, and atmospheric forcing during mooring-Argo period is comparable to the longer-term variability. These time series enable us to interpret recent Irminger Sea observations in the context of large variability previously identified on decadal time scales (Chafik et al., 2022; Josey et al., 2019; van Aken et al., 2011). Van Aken et al. (2011), describing the survey record up to 2010, identified six events with low PV and high dissolved oxygen concentrations at 1,500 dbar, a typical signature of convectively ventilated water masses. In the extended record, the 1990s event stands out as the strongest convection event (Figure 2), producing a particularly thick cold, fresh and dense water mass ($27.75 < \sigma_0 < 27.8$ kg m^{-3}). The more recent low PV signal, initiated with the strong convection in the winter of 2014–2015 is shallower than that observed in the 1990s. The shallower convection resulted in densities in the 500–1,000 m layer that are less dense than seen in the 1990s and more like those seen in the 1970s and 1980s ($27.7 < \sigma_0 < 27.75$ kg m^{-3}).

The 19-year mooring-Argo record gives insight into the range of interannual variability in convection, with MLD reaching only 288 dbar in 09–10 and as deep as 1,500 dbar in 14–15. Mixed layers shallower than 500 dbar do not leave an imprint on the local PV profile, as this layer is completely restratified through spring and summer, but deeper mixed layers do. Both the observations and simulations with the PWP MLD model indicate that the depth of convection is determined mainly by the strength of the atmospheric buoyancy forcing in winter, with a maximum around 1,500 dbar because of an increased deep density gradient associated with the transition to overflow waters. Winters with very shallow convection after strong stratification (03–04, 09–10, and 18–19) also coincided with weaker than average atmospheric forcing. Both the mooring-Argo data and the PWP experiments show that the interannual variability in the strength of the atmospheric forcing largely determines the observed changes in convection depth over the 2002–2020 period. The convection depth is not significantly correlated to the stratification in the preceding summer. This result agrees with findings of Kim et al. (2021), who posited that weak convection during a GSA in the Labrador Sea was also mainly caused by weak atmospheric forcing. However, the fresh anomaly arriving in the Irminger Sea toward the end of the mooring record (Bilo et al., 2022; de Jong et al., 2020; Holliday et al., 2020) does have an effect on the hydrography, as these fresh waters are mixed into the water column and freshened the waters at intermediate depths (Fried et al., 2024). Despite the lower salinities, the cold character of the strong convection from 2014 to 2018 created a class of middepth waters in the Irminger Sea that is the densest in the 19-year record.

The timing of the return of convection in the winter of 14–15 is auspicious, as this was also the first winter observed by the OSNAP array and the OOI moorings. However, the sudden transition from a warm, buoyant and high ADT period to a period of cold, dense and low ADT preceded the addition of these new observations. This makes the long-term context provided by the new 2002–2020 weekly time-series presented here especially critical to contextualize analyses of OSNAP and OOI data. Since convection has weakened after 2018, it is likely that the Irminger Sea will return to a warm, buoyant period, but this restratification is much more gradual (Nelson et al., 2024). The overturning at OSNAP East is related to water mass transformation of all buoyant waters to waters denser than 27.53 kg m^{-3} (Li et al., 2021; Lozier et al., 2019; Petit et al., 2020). The convection at the mooring locations in the CIS adds mainly to the densest waters formed at OSNAP East (Petit et al., 2020), however the atmospheric forcing driving the variability at this location is coherent over a much wider area (Josey et al., 2019). Mixing along the boundaries (Le Bras et al., 2020, 2022) as well as shallower mixing over more stratified waters further east (de Jong et al., 2020) will contribute to the total overturning in lighter density classes. The weak stratification in the cyclonic Irminger Gyre makes this area especially sensitive to the interannual variability in surface forcing caused by the Greenland Tip Jet. This is reflected in the minimum in ADT identified as a center of action for the Subpolar Gyre by Chafik et al. (2022), which we here find is related mainly to local convection and not to the advection of intermediate waters from elsewhere. Continued measurements in the CIS will be essential to understanding overturning in the Subpolar Gyre.

We showed that in the past 19 years of the Irminger Sea, and likely the last 70, the forcing was always strong enough to penetrate the initial stratification of the upper layer. Once the stratification over the upper layer is removed the middepth layer is relatively easy to homogenize until the transition to overflow derived waters at 1,500 m is reached. Additionally, we found that the maximum stratification in summer relies strongly on

convection in the previous winter. This agrees with the finding of Sterl and de Jong (2022) that there is little interannual variability in the strength of restratification over the upper 600 m in the Irminger Sea. This gives the atmospheric forcing additional importance as it sets both the strength of convection in the current year as well as the next. Under climate change, the stratification of the Irminger Sea is projected to strengthen as a result of a warming upper ocean and an increase in freshwater input (Bakker et al., 2016; Sgubin et al., 2017). Conditions such as in 2010 and 2019 are likely to become more prevalent, moving the Irminger Sea to the edge of the currently observed parameter space in terms of stratification. Under those conditions, convection could shallow by 170 m on average, but deep MLDs of up to 1,200 m could still occur under strong forcing (Figure 7e). In those cases, stratification would be significantly reduced for the subsequent years, possibly allowing deep convection to return again under somewhat weaker forcing (similar to 08–09 in Figure 5 and de Jong et al., 2012). However, once the stratification becomes stronger than observed thus far, its impact may be larger. Nevertheless, future forcing conditions are likely to change as well. For example, less frequent occurrences of tip jets due to a shift in the jet stream or a warmer atmosphere and reduced air-sea temperature difference (Fedorov et al., in revision) could significantly reduce heat loss and thereby weaken MLD more substantially than an increase in stratification. Therefore, changes in atmospheric forcing need to be taken into account when considering changes in convection.

Data Availability Statement

Data from LOCO deployments between 2003 and 2011 are available from the OceanSITES repository at https://www.ndbc.noaa.gov/data/oceansites/deployment_data/LOCO-IRMINGSEA/. Data from LOCO deployments between 2012 and 2018 are available at (de Jong, 2023a, 2023b, 2023c, 2023d, 2023e). Quality controlled OOI profile data used in this study is available at (Le Bras, 2023). Data from ERA5 (Hersbach et al., 2018) were obtained from https://cds.climate.copernicus.eu/datasets/reanalysis-era5-single-levels?tab=overview.

Acknowledgments
MFdJ is financially supported by the Innovational Research Incentives Scheme of the Netherlands Organisation for Scientific Research (NWO) under grant agreement nos. 016.Vidi.189.130. KEF and HIP were supported by the US National Science Foundation (NSF) under award #1946072. ILB was supported by the NSF under awards OCE-2038481 and OCE- 2122579. The authors thank the many research vessels and crews that have contributed to the collection of these data from different programs over the last 70 years. Thanks to Johannes Karstensen for the CIS data. The Long-term Ocean-Climate Observations (LOCO) program was started in 2003 as a NWO financed large investment program (NWO Groot), of which the CIS mooring was one component. This particular LOCO mooring was continued as part of the European Community's 7th Framework Programme (FP7/2007–2013) under grant agreement No. GA212643 (THOR: "Thermohaline Overturning—at Risk," 2008–2012), European Union 7th Framework Programme (FP7 2007–2013) under grant agreement n.308299 NACLIM in 2012 and finally under the Horizon 2020 Research and Innovation Program under Grant 727852 (Blue-Action) in 2016. Occasional gaps between funding sources were covered by the Royal Netherlands Institute for Sea Research (NIOZ). The CIS Mooring received funding by the EU FP5 ANIMATE (EVR1-CT-2001-40014), EU FP6 MERSEA (502885), EU FP7 EuroSITES (202955), EU FP7 FixO3 (312463), EU FP7 NACLIM (308299), BMBF Nordatlantik, BMBF RACE, Deutsche Forschungsgemeinschaft within the METEOR/MERIAN core program. Ocean Observatories Initiative is a major facility fully funded by the NSF under Cooperative Agreement No. 1743430, and the Woods Hole Oceanographic Institution OOI Program Office. Argo data were collected and made freely available by the International Argo Program and the national programs that contribute to it (https://argo.ucsd.edu, https://www.ocean-ops.org). The Argo Program is part of the Global Ocean Observing System.

References

Bakker, P., Schmittner, A., Lenaerts, J. T. M., Abe-Ouchi, A., Bi, D., van den Broeke, M. R., et al. (2016). Fate of the Atlantic meridional overturning circulation: Strong decline under continued warming and Greenland melting. *Geophysical Research Letters*, *43*(23), 12252–12260. https://doi.org/10.1002/2016GL070457

Belkin, I. M., Levitus, S., Antonov, J. I., & Malmberg, S.-A. (1998). "Great Salinity Anomalies" in the North Atlantic. *Progress in Oceanography*, *41*, 1–68. https://doi.org/10.1016/S0079611(98)00015-9

Biló, T. C., Straneo, F., Holte, J., & Le Bras, I. A.-A. (2022). Arrival of new Great Salinity Anomaly weakens convection in the Irminger Sea. *Geophysical Research Letters*, *49*(11), e2022GL098857. https://doi.org/10.1029/2022GL098857

Böning, C. W., Behrens, E., Biastoch, A., Getzlaff, K., & Bamber, J. L. (2016). Emerging impact of Greenland meltwater on deepwater formation in the North Atlantic Ocean. *Nature Geoscience*, *9*(7), 523–527. https://doi.org/10.1038/ngeo2740

Böning, C. W., Scheinert, M., Dengg, J., Biastoch, A., & Funk, A. (2006). Decadal variability of subpolar gyre transport and its reverberation in the North Atlantic overturning. *Geophysical Research Letters*, *33*(21), L21S01. https://doi.org/10.1029/2006GL026906

Chafik, L., Holliday, N. P., Bacon, S., & Rossby, T. (2022). Irminger Sea is the center of action for subpolar AMOC variability. *Geophysical Research Letters*, *49*(17). https://doi.org/10.1029/2022GL099133

de Jong, M. F. (2023a). Hydrography and velocity data from the Long-term Ocean Circulation Observations (LOCO) mooring in the central Irminger Sea: Deployment nine (LOCO2_9) July 2011 to August 2012 (Version 1) [Dataset]. https://doi.org/10.25850/nioz/7b.b.mg

de Jong, M. F. (2023b). Hydrography and velocity data from the Long-term Ocean Circulation Observations (LOCO) mooring in the central Irminger Sea: Deployment ten (LOCO2_10) August 2012 to July 2014 (Version 1) [Dataset]. https://doi.org/10.25850/nioz/7b.b.ng

de Jong, M. F. (2023c). Hydrography and velocity data from the Long-term Ocean Circulation Observations (LOCO) mooring in the central Irminger Sea: Deployment eleven (LOCO2_11) September 2014 to July 2015 (Version 1) [Dataset]. https://doi.org/10.25850/nioz/7b.b.pg

de Jong, M. F. (2023d). Hydrography and velocity data from the Long-term Ocean Circulation Observations (LOCO) mooring in the central Irminger Sea: Deployment twelve (LOCO2_12) July 2015 to August 2016 (Version 1) [Dataset]. https://doi.org/10.25850/nioz/7b.b.qg

de Jong, M. F. (2023e). Hydrography and velocity data from the Long-term Ocean Circulation Observations (LOCO) mooring in the central Irminger Sea: Deployment thirteen (LOCO2_13) August 2016 to June 2018 (Version 1) [Dataset]. https://doi.org/10.25850/nioz/7b.b.rg

de Jong, M. F., & de Steur, L. (2016). Strong winter cooling over the Irminger Sea in winter 2014–2015, exceptional deep convection, and the emergence of anomalously low SST. *Geophysical Research Letters*, *43*(13), 7106–7113. https://doi.org/10.1002/2016GL069596

de Jong, M. F., Oltmanns, M., Karstensen, J., & de Steur, L. (2018). Deep convection in the Irminger Sea observed with a dense mooring array. *Oceanography*, *31*(1), 50–59. https://doi.org/10.5670/oceanog.2018.109

de Jong, M. F., Steur, L., Fried, N., Bol, R., & Kritsotalakis, S. (2020). Year-round measurements of the Irminger current: Variability of a two-core current system observed in 2014–2016. *Journal of Geophysical Research: Oceans*, *125*(10), e2020JC016193. https://doi.org/10.1029/2020JC016193

de Jong, M. F., van Aken, H. M., Våge, K., & Pickart, R. S. (2012). Convective mixing in the central Irminger Sea: 2002–2010. *Deep Sea Research I*, *63*, 36–51. https://doi.org/10.1016/j.dsr.2012.01.003

Dickson, R. R., Meincke, J., Malmberg, S.-A., & Lee, A. J. (1988). The "great salinity anomaly" in the Northern North Atlantic 1968–1982. *Progress in Oceanography*, *20*(2), 103–151. https://doi.org/10.1016/0079-6611(88)90049-3

Duyck, E., Gelderloos, R., & de Jong, M. F. (2022). Wind-driven freshwater export at Cape Farewell. *Journal of Geophysical Research: Oceans*, *127*(5), e2021JC018309. https://doi.org/10.1029/2021JC018309

Eden, C., & Willebrand, J. (2001). Mechanism of Interannual to decadal variability of the North Atlantic circulation. *Journal of Climate*, *14*(10), 226–2280. https://doi.org/10.1175/1520-0442(2001)014%3C2266:MOITDV%3E2.0.CO;2

21699291, 2025, 2, Downloaded from https://agupubs.onlinelibrary.wiley.com/doi/10.1029/2023JC020799, Wiley Online Library on [31/01/2025]. See the Terms and Conditions (https://onlinelibrary.wiley.com/terms-and-conditions) on Wiley Online Library for rules of use; OA articles are governed by the applicable Creative Commons License

Fedorov, A. M., Wieners, C. E., de Jong, M. F., & Dijkstra, H. A. (in revision). Understanding the Greenland tip jet role in the future: Declining Surface Heat Loss in a High-resolution CESM simulation (2015-2099). *Submitted to Journal of Climate*.

Fried, N., Carrilho Biló, T., Johns, W. J., Katsman, C., Fogaren, K., Yoder, M., et al. (2024). Freshening over the whole water column as a result of the 2012 subpolar freshwater anomaly increased the transport of lighter waters of the Irminger Current between 2014 - 2022. *Submitted to Journal of Geophysical Research – Oceans*, *129*(11), e2024JC021184. https://doi.org/10.1029/2024JC021184

Gelderloos, R., Straneo, F., & Katsman, C. A. (2012). Mechanisms behind the temporary shutdown of deep convection in the Labrador Sea: Lessons from the Great Salinity Anomaly Years 1968–71. *Journal of Climate*, *25*(19), 6743–6755. https://doi.org/10.1175/jcli-d-11-00549.1

Hersbach, H., Bell, B., Berrisford, P., Biavati, G., Horányi, A., Muñoz Sabater, J., et al. (2018). ERA5 hourly data on single levels from 1959 to present [Dataset]. *Copernicus Climate Change Service (C3S) Climate Data Store (CDS)*. https://doi.org/10.24381/cds.adbb2d47

Holliday, P. N., Bersch, M., Berx, B., Chafik, L., Cunningham, S., Florindo-López, C., et al. (2020). Ocean circulation causes the largest freshening event for 120 years in eastern Subpolar North Atlantic. *Nature Communications*, *11*(1), 585. https://doi.org/10.1038/s41467-020-14474-y

Holte, J., & Straneo, F. (2017). Seasonal overturning of the Labrador Sea as observed by Argo floats. *Journal of Physical Oceanography*, *47*(10), 2531–2543. https://doi.org/10.1175/JPO-D17-0051.1

Jerlov, N. G. (1968). *Optical oceanography* (p. 194). Elsevier.

Josey, S. A., de Jong, M. F., Oltmanns, M., Moore, G. K., & Weller, R. A. (2019). Extreme variability in Irminger Sea winter heat loss revealed by Ocean Observatories Initiative mooring and the ERA5. Reanalysis. *Geophysical Research Letters*, *46*(1), 293–302. https://doi.org/10.1029/2018GL080956

Katsman, C. A., Drijfhout, S. S., Dijkstra, H. A., & Spall, M. A. (2018). Sinking of dense North Atlantic waters in a global ocean model: Location and controls. *Journal of Geophysical Research: Oceans*, *123*(5), 3563–3576. https://doi.org/10.1029/2017JC013329

Kim, W. M., Yeager, S., & Danabasoglu, G. (2021). Revisiting the causal connection between the Great Salinity Anomaly of the 1970s and the shutdown of Labrador Sea deep convection. *Journal of Climate*, *34*(2), 675–696. https://doi.org/10.1175/JCLI-D-20-0327.1

Lazarevich, P., Rossby, T., & McNeil, C. (2004). Oxygen variability in the near-surface waters of the northern North Atlantic: Observations and a model. *Journal of Marine Research*, *62*(5), 663–683. https://doi.org/10.1357/0022240042387547

Lazier, J. R. N. (1980). Oceanographic conditions at Ocean Weather Ship Bravo, 1964–1974. *Atmosphere-Ocean*, *18*(3), 227–238. https://doi.org/10.1080/07055900.1980.9649089

Le Bras, I. (2023). Potential temperature and salinity profiles from the Ocean Observatories Initiative Global Irminger Sea Array Apex profiler mooring from September 2014 to May 2020 (NCEI Accession 0285241) NOAA National Centers for Environmental Information. [Dataset]. https://www.ncei.noaa.gov/archive/accession/0285241

Le Bras, I. A.-A., Callies, J., Straneo, F., Biló, T. C., Holte, J., & Johnson, H. L. (2022). Slantwise Convection in the Irminger Sea. *Journal of Geophysical Research: Oceans*, *127*, e2022JC019071. https://doi.org/10.1029/2022jc019071

Le Bras, I. A.-A., Straneo, F., Holte, J., de Jong, M. F., & Holliday, N. P. (2020). Rapid export of waters formed by convection near the Irminger Sea's western boundary. *Geophysical Research Letters*, *47*(3), e2019GL085989. https://doi.org/10.1029/2019GL085989

Li, F., Lozier, M. S., Bacon, S., Bower, A. S., Cunningham, S. A., de Jong, M. F., et al. (2021). Subpolar North Atlantic western boundary density anomalies and the Meridional Overturning Circulation. *Nature Communications*, *12*(1), 3002. https://doi.org/10.1038/s41467-021-23350-2

Lozier, M. S., Bacon, S., Bower, A. S., Cunningham, S. A., de Jong, M. F., de Steur, L., et al. (2017). Overturning in the Subpolar North Atlantic Program: A new international ocean observing system. *Bulletin of the American Meteorological Society*, *98*(4), 737–752. https://doi.org/10.1175/BAMS-D-16-0057.1

Lozier, S. M., Li, F., Bacon, S., Bahr, F., Bower, A. S., Cunningham, S. A., et al. (2019). A sea change in our view of Overturning in the Subpolar North Atlantic. *Science*, *363*(6426), 516–521. https://doi.org/10.1126/science.aau6592

Marshall, J., & Schott, F. (1999). Open ocean deep convection: Observations, models and theory. *Reviews of Geophysics*, *37*, 1–64. https://doi.org/10.1029/98RG02739

Moore, G. W. K. (2003). Gale force winds over the Irminger Sea to the east of Cape Farewell, Greenland. *Geophysical Research Letters*, *30*(17), 1894. https://doi.org/10.1029/2003GL018012

Moore, G. W. K., & Renfrew, I. A. (2005). Tip jets and barrier winds: A QuickSCAT climatology of high wind speed events around Greenland. *Journal of Climate*, *18*, 3713–3725. https://doi.org/10.1175/JCLI3455.1

Mulet, S., Rio, M.-H., Mignot, A., Guinehut, S., & Morrow, R. (2012). A new estimate of the global 3D geostrophic ocean circulation based on satellite data and in-situ measurements. *Deep Sea Research Part II*, *77–80*(0), 70–81. https://doi.org/10.1016/j.dsr2.2012.04.012

Nansen, F. (1912). Das Bodenwasser und die Abkuhlung des Meeres. *Internationale Revue der gesamten Hydrobiologie und Hydrographie*, *5*, 1–42. https://doi.org/10.1002/iroh.19120050102

Nelson, M., Straneo, F., Purkey, S. G., & de Jong, M. F. (2024). Delayed recovery of the Irminger interior from cooling in 2015 due to widespread buoyancy loss and suppressed restratification. *Geophysical Research Letters*, *51*(2), e2023GL106501. https://doi.org/10.1029/2023GL106501

Oltmanns, M., Karstensen, J., & Fischer, J. (2018). Increased risk of a shutdown of ocean convection posed by warm North Atlantic summers. *Nature Climate Change*, *8*(4), 300–304. https://doi.org/10.1038/s41558-018-0105-1

Paulson, C. A., & Simpson, J. J. (1977). Irradiance measurements in the Upper Ocean. *Journal of Physical Oceanography*, *7*(6), 952–956. https://doi.org/10.1175/1520-0485(1977)007<0952:IMITUO>2.0.CO;2

Petit, T., Lozier, M. S., Josey, S. A., & Cunningham, S. A. (2020). Atlantic deep water formation occurs primarily in the Iceland Basin and Irminger Sea by local buoyancy forcing. *Geophysical Research Letters*, *47*(22), e2020GL091028. https://doi.org/10.1029/2020GL091028

Pickart, R. S., Straneo, F., & Moore, G. W. K. (2003). Is Labrador Sea Water formed in the Irminger Basin? *Deep Sea Research I*, *50*(1), 23–52. https://doi.org/10.1016/S09670637(02)00134-6

Piron, A., Thierry, V., Mercier, H., & Caniaux, G. (2015). Observations of basin scale deep convection in the Irminger Sea with Argo floats in the winter of 2011-2012. *Deep-Sea Research I*, *109*, 76–90. https://doi.org/10.1016/j.dsr.2015.12.012

Piron, A., Thierry, V., Mercier, H., & Caniaux, G. (2017). Gyre-scale deep convection in the subpolar North Atlantic Ocean during winter 2014–2015. *Geophysical Research Letters*, *44*(3), 1439–1447. https://doi.org/10.1002/2016GL071895

Price, J. F., Weller, R. A., & Pinkel, R. (1986). Diurnal cycling: Observations and models of the upper ocean response to diurnal heating, cooling, and wind mixing. *Journal of Geophysical Research*, *91*(C7), 8411–8427. https://doi.org/10.1029/JC091iC07p08411

Renfrew, I. A., Barrell, C., Elvidge, A. D., Brooke, J. K., Duscha, C., King, J. C., et al. (2021). An evaluation of surface meteorology and fluxes over the Iceland and Greenland Seas in ERA5 reanalysis: The impact of sea ice distribution. *Quarterly Journal of the Royal Meteorological Society*, *147*(734), 691–712. https://doi.org/10.1002/qj.3941

Schmidt, S., & Send, U. (2007). Origin and composition of seasonal Labrador Sea freshwater. *Journal of Physical Oceanography*, *37*(6), 1445–1454. https://doi.org/10.1175/JPO3065.1

21699291, 2025, 2, Downloaded from https://agupubs.onlinelibrary.wiley.com/doi/10.1029/2023JC020799, Wiley Online Library on [31/01/2025]. See the Terms and Conditions (https://onlinelibrary.wiley.com/terms-and-conditions) on Wiley Online Library for rules of use; OA articles are governed by the applicable Creative Commons License

Sgubin, G., Swingedouw, D., Drijfhout, S., Mary, Y., & Bennabi, A. (2017). Abrupt cooling over the North Atlantic in modern climate models. *Nature Communications*, *8*(1), 14375. https://doi.org/10.1038/ncomms14375

Sterl, M. F., & de Jong, M. F. (2022). Restratification structure and processes in the Irminger Sea. *Journal of Geophysical Research: Oceans*, *127*(12), e2022JC019126. https://doi.org/10.1029/2022jc019126

Straneo, F. (2006). On the connection between dense water formation, overturning, and poleward heat transport in a convective basin. *Journal of Physical Oceanography*, *36*(9), 1822–1840. https://doi.org/10.1175/JPO2932.1

Sverdrup, H. U., Johnson, M. W., & Fleming, R. H. (1942). *The Oceans: Their physics, chemistry, and general biology*. Prentice-Hall Inc. 1060.

van Aken, H. M., de Jong, M. F., & Yashayaev, I. (2011). Decadal and multi-decadal variability of Labrador Sea water in the north-western North Atlantic Ocean derived from tracer distributions: Heat budget, ventilation, and advection. *Deep-Sea Research I*, *58*, 505–523. https://doi.org/10.1016/j.dsr.2011.02.008

Woods, R. A., Keen, A. B., Mitchell, J. F., & Gregory, J. M. (1999). Changing spatial structure of the thermohaline circulation in response to atmospheric CO2 forcing in a climate model. *Nature*, *399*(6736), 572–575. https://doi.org/10.1038/21170

Yashayaev, I. (2007). Hydrographic changes in the Labrador Sea, 1960–2005. *Progress in Oceanography*, *73*(3–4), 242–276. https://doi.org/10.1016/j.pocean.2007.04.015

Zhang, R., Sutton, R., Danabasoglu, G., Kwon, Y.-O., Marsh, R., Yeager, S. G., et al. (2019). A review of the role of the Atlantic meridional overturning circulation in Atlantic multidecadal variability and associated climate impacts. *Reviews of Geophysics*, *57*(2), 316–375. https://doi.org/10.1029/2019RG000644

21699291, 2025, 2, Downloaded from https://agupubs.onlinelibrary.wiley.com/doi/10.1029/2023JC020799, Wiley Online Library on [31/01/2025]. See the Terms and Conditions (https://onlinelibrary.wiley.com/terms-and-conditions) on Wiley Online Library for rules of use; OA articles are governed by the applicable Creative Commons License